



Quantum-mimetic imaging

DHEERA VENKATRAMAN
29 JANUARY 2015 | THESIS DEFENSE



Massachusetts
Institute of
Technology

Outline

1. **Overview:** Quantum metrology and quantum-mimetic imaging
2. **Experiment:** PC-OCT
3. **Experiment:** Classical phase-sensitive ghost imaging
4. **Experiment:** First-photon imaging
5. **Conclusions**

1 OVERVIEW

Quantum vs. quantum-mimetic imaging

What is quantum metrology?

Experiments that exploit quantum states of light (e.g. entangled states)

Experiments that use quantum detection methods

Cannot be explained by semiclassical theory

Example: Q-OCT

Quantum optical coherence tomography

Uses an entangled biphoton source

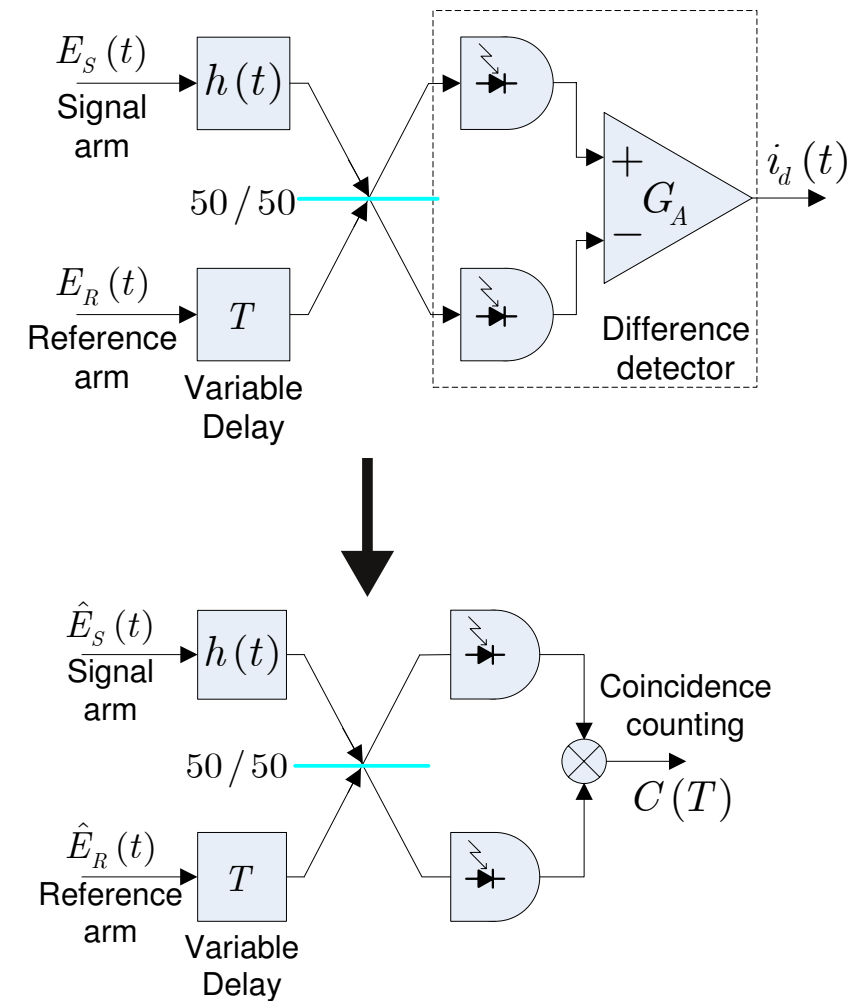
Advantages

Factor-of-2 resolution improvement
and even-order dispersion cancellation

Advantages initially attributed to quantum physics

M. B. Nasr et al., Phys. Rev. Lett. 91, 083601 (2003)

B. I. Erkmen and J. H. Shapiro. Phys. Rev. A, 74:041601 (2006)



Example: Ghost imaging

Ghost imaging

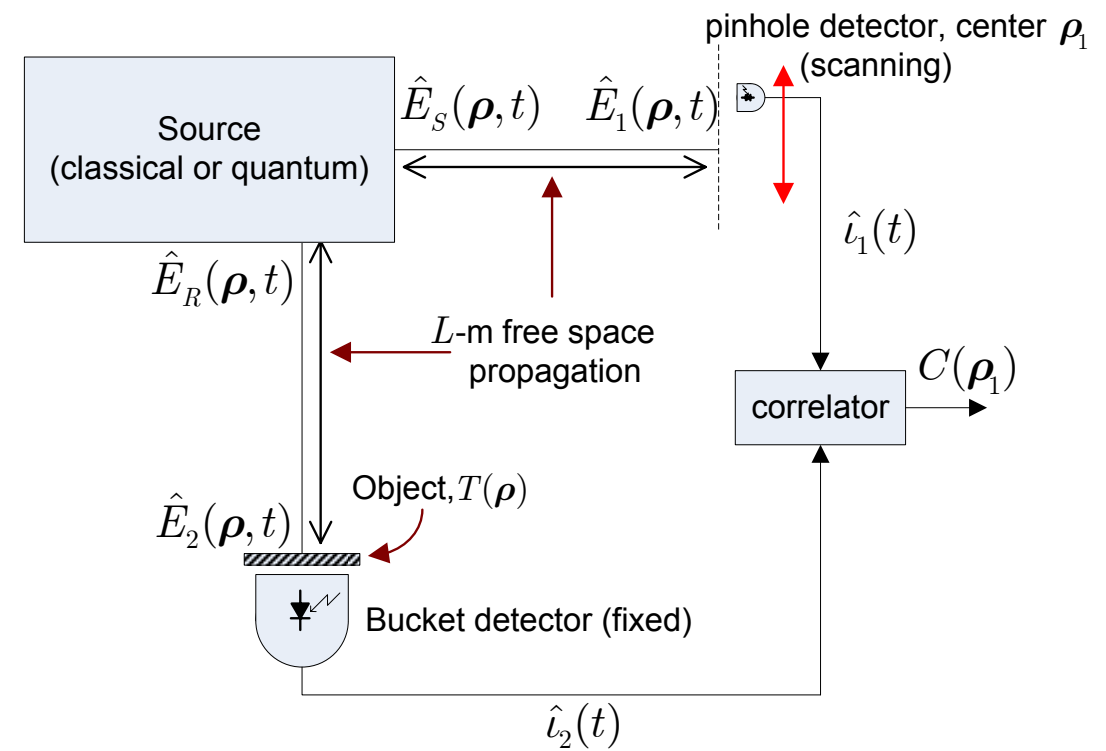
Uses an entangled biphoton source

Advantages

Images at wavelengths without CCDs

Signal arm only requires a single detector

Initially thought to be uniquely quantum



Quantum-mimetic imaging

Quantum imaging experiments are explained by quantum theories, but their claimed advantages may not necessarily be uniquely quantum.

Quantum-mimetic imaging experiments use non-traditional, classical setups to achieve results similar to their quantum counterparts.

2 EXPERIMENT

Phase-conjugate optical coherence tomography

Motivation

Q-OCT advantages (even-order dispersion cancellation, factor-of-2 resolution improvement) shown to originate from phase-sensitive cross-correlations between signal and idler and **not entanglement**

PC-OCT employs a classical phase-sensitive source which is **maximally correlated in the classical sense**

Phase-sensitive vs. Phase-insensitive

Phase-insensitive auto-correlations:

$$K_{SS}^{(n)}(\tau) = \langle E_S^*(t)E_S(t + \tau) \rangle$$

$$K_{RR}^{(n)}(\tau) = \langle E_R^*(t)E_R(t + \tau) \rangle$$

Phase-insensitive cross-correlations:

$$K_{SR}^{(n)}(\tau) = \langle E_S^*(t)E_R(t + \tau) \rangle$$

Phase-sensitive cross-correlations:

$$K_{SR}^{(p)}(\tau) = \langle E_S(t)E_R(t + \tau) \rangle$$

Cauchy-Schwarz bound for classical states:

$$|S_{SR}^{(p)}(\Omega)| \leq \sqrt{S_{SS}^{(n)}(-\Omega)S_{RR}^{(n)}(\Omega)}$$

Equality satisfied by: $K_{SS}^{(n)}(\tau) = K_{RR}^{(n)}(\tau) = K_{SR}^{(n)}(\tau)$

$$|S_{SR}^{(n)}(\Omega)| \leq \sqrt{S_{SS}^{(n)}(\Omega)S_{RR}^{(n)}(\Omega)}$$

Equality satisfied by: $K_{SS}^{(p)}(\tau) = K_{RR}^{(p)}(\tau) = K_{SR}^{(p)}(\tau)$

Coherence theory for classical states

Maximally-entangled quantum states can violate Cauchy-Schwarz:

$$K_{SS}^{(n)}(\tau) = \langle \hat{E}_S^\dagger(t) \hat{E}_S(t + \tau) \rangle$$

$$K_{RR}^{(n)}(\tau) = \langle \hat{E}_R^\dagger(t) \hat{E}_R(t + \tau) \rangle$$

$$K_{SR}^{(p)}(\tau) = \langle \hat{E}_S^\dagger(t) \hat{E}_R(t + \tau) \rangle$$

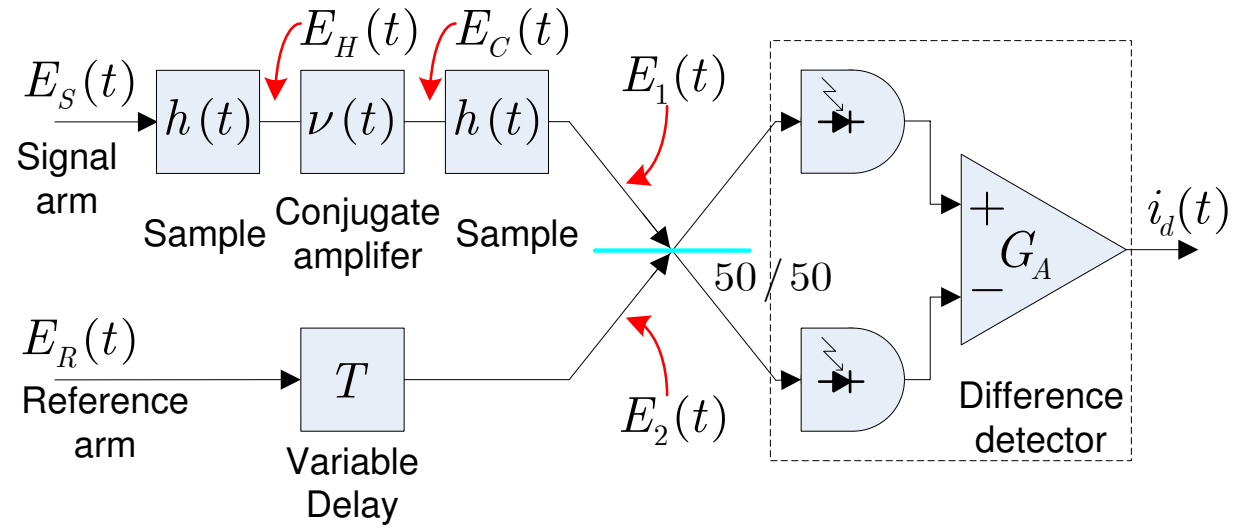
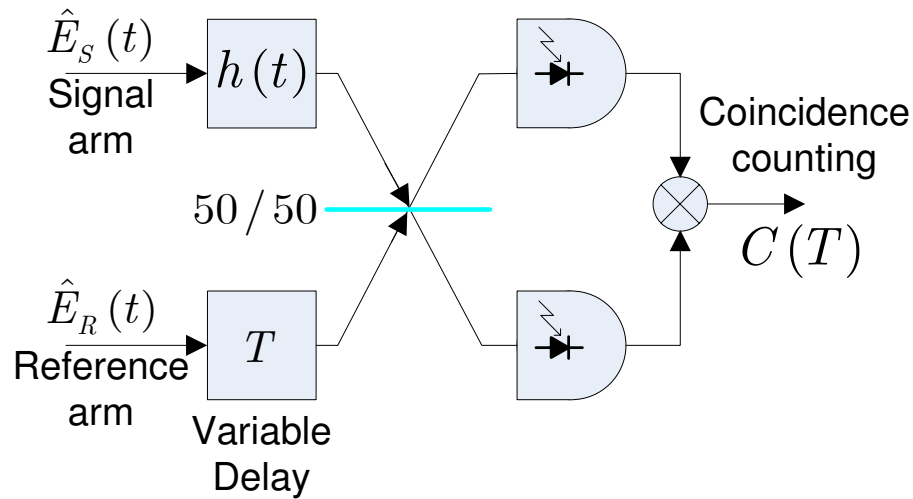
$$K_{SS}^{(n)}(\tau) = K_{RR}^{(n)}(\tau) = \int_{-\infty}^{\infty} \frac{d\Omega}{2\pi} S(\Omega) e^{-i\Omega\tau}$$

$$K_{SR}(\tau) = \int_{-\infty}^{\infty} \frac{d\Omega}{2\pi} \sqrt{S(\Omega)(S(\Omega) + 1)} e^{-i\Omega\tau}$$

Quantum states not necessary to achieve dispersion cancellation and factor-of-2 resolution improvement.

Schematic

PC-OCT uses classical phase-sensitive light and a double-pass configuration to obtain similar advantages to Q-OCT



Comparison of interference signatures

C-OCT signature

$$\langle i_d(t) \rangle = 2q\eta G_A \operatorname{Re} \left(\int_{-\infty}^{\infty} \frac{d\Omega}{2\pi} H^*(-\Omega) S(\Omega) e^{-i(\Omega - \omega_0)T} \right) \quad H(\Omega) = r e^{i(\omega_0 + \Omega)T_0 + \beta(\Omega)}$$

Q-OCT signature

$$\langle C(T) \rangle = \frac{q^2 \eta^2}{2} \left[\int_{-\infty}^{\infty} \frac{d\Omega}{2\pi} |H(\Omega)|^2 S(\Omega) - \operatorname{Re} \left(\int_{-\infty}^{\infty} \frac{d\Omega}{2\pi} H^*(-\Omega) H(\Omega) S(\Omega) e^{-2i\Omega T} \right) \right]$$

PC-OCT signature

$$\langle i_d(t) \rangle = 2q\eta G_A \operatorname{Re} \left(\int_{-\infty}^{\infty} \frac{d\Omega}{2\pi} H^*(-\Omega) H(\Omega) \times V^*(-\Omega) S(\Omega) e^{-i(\Omega - \omega_0)T} \right)$$

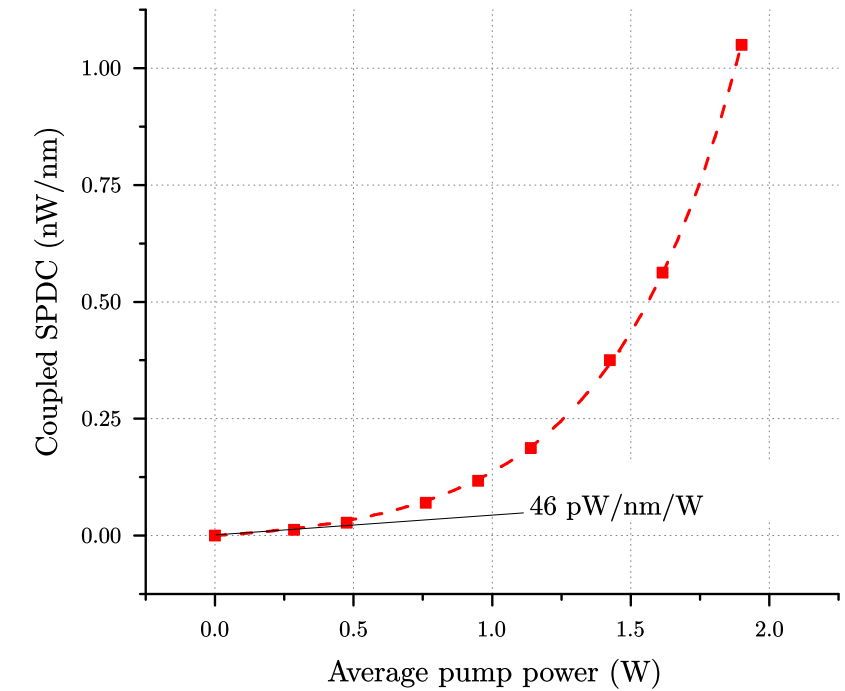
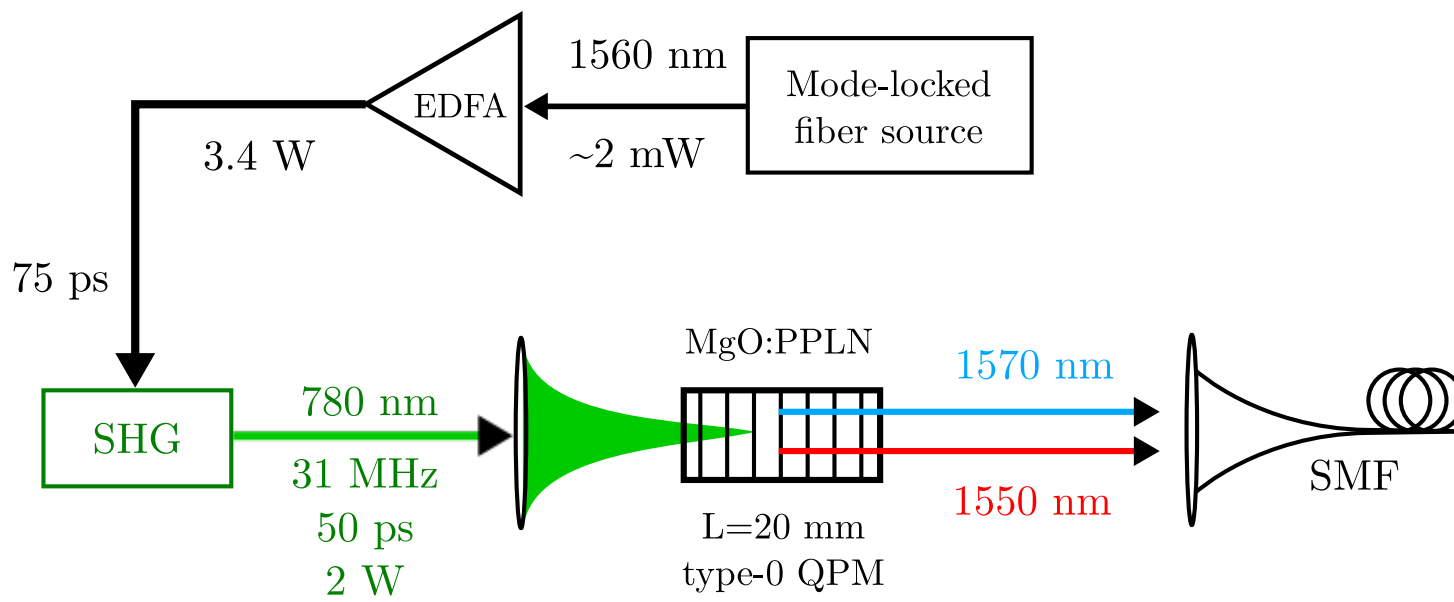


"Quantum-mimetic"

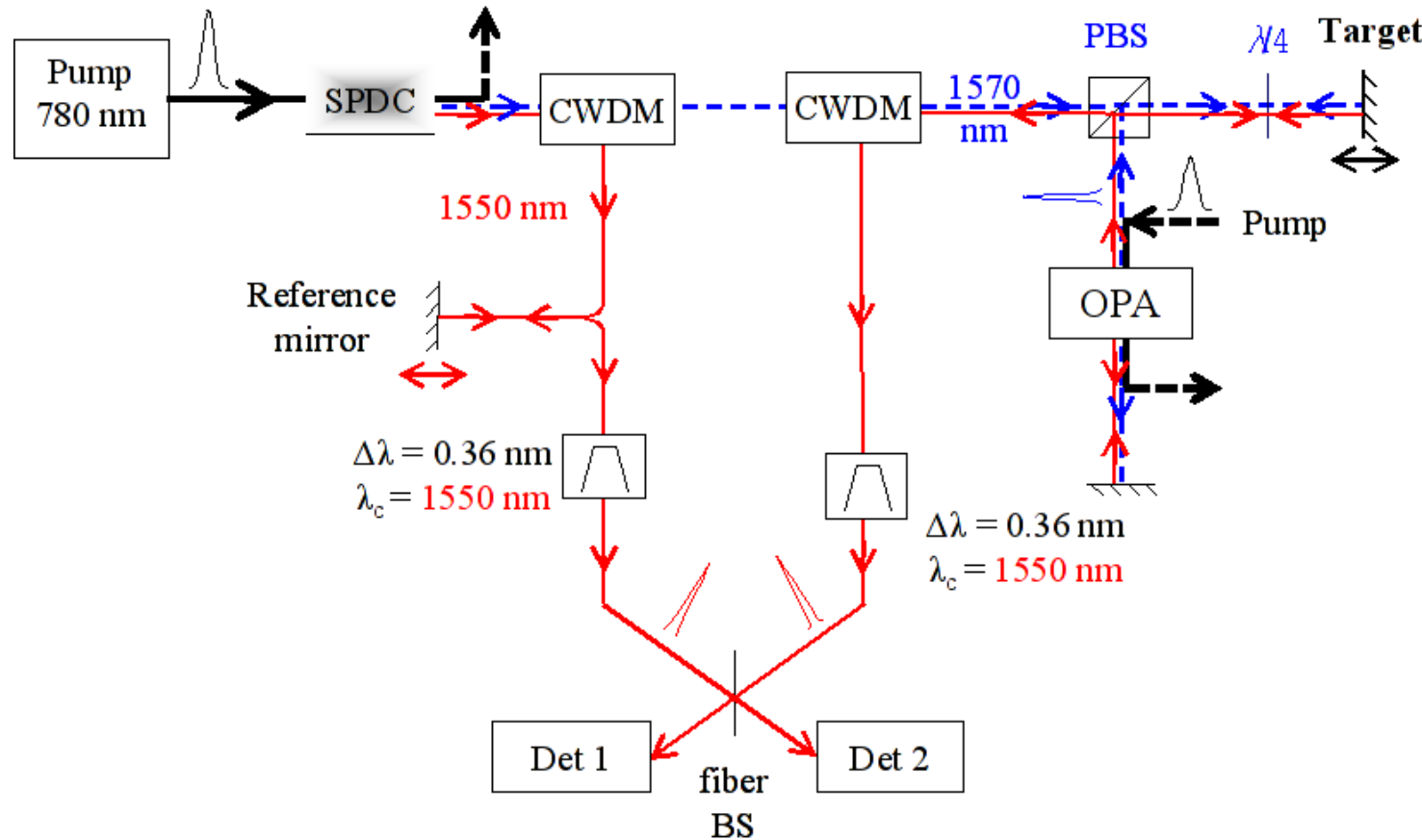
Classical phase-sensitive light source

Amplified SPDC used to signal and idler beams

Entanglement-breaking; maximally classically correlated



PC-OCT setup



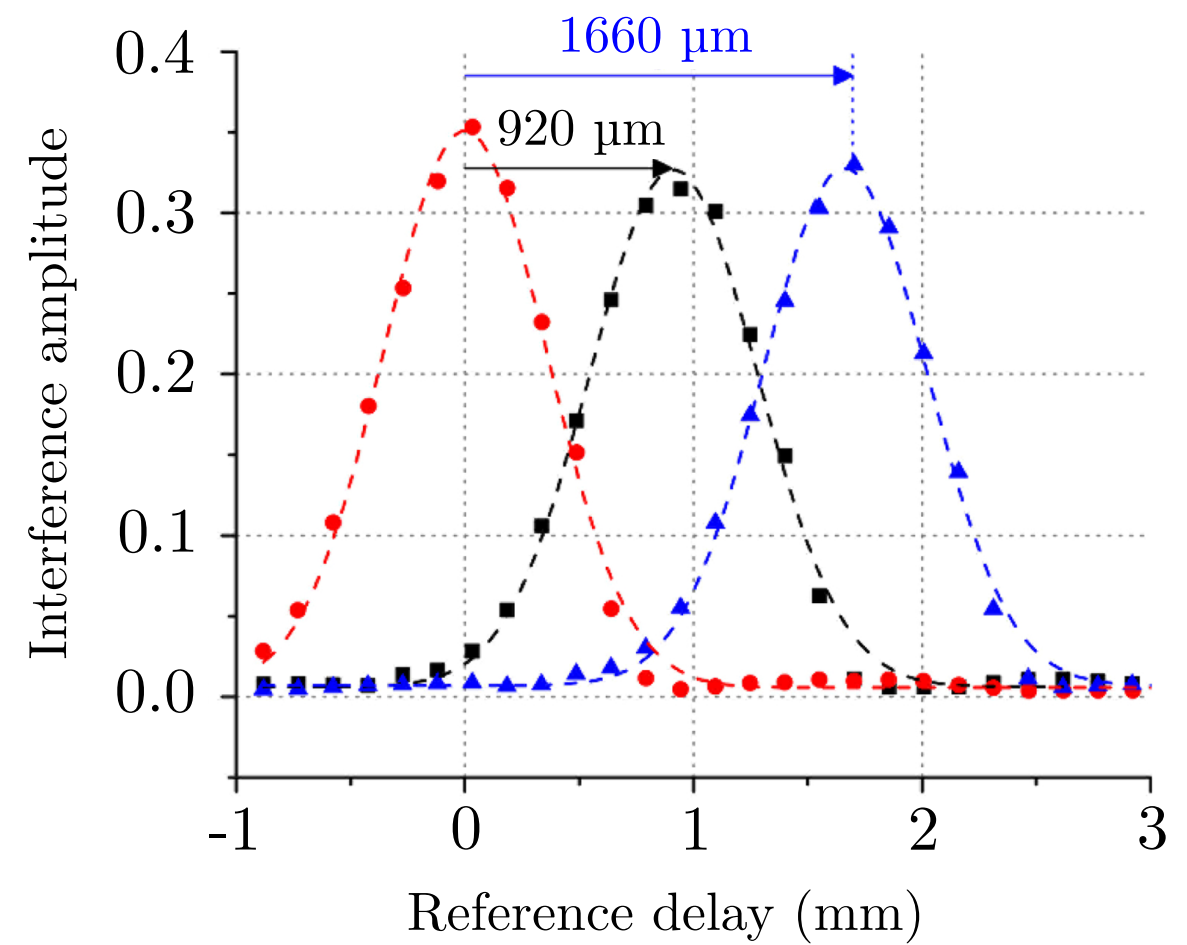
Results

Translation steps of 450 μm

Factor-of-2 resolution improvement visible

Dispersion cancelled almost perfectly

Temperature fluctuations affected long fibers



3 EXPERIMENT

Far-field phase-sensitive ghost imaging

Ghost imaging history

PHYSICAL REVIEW A

VOLUME 52, NUMBER 5

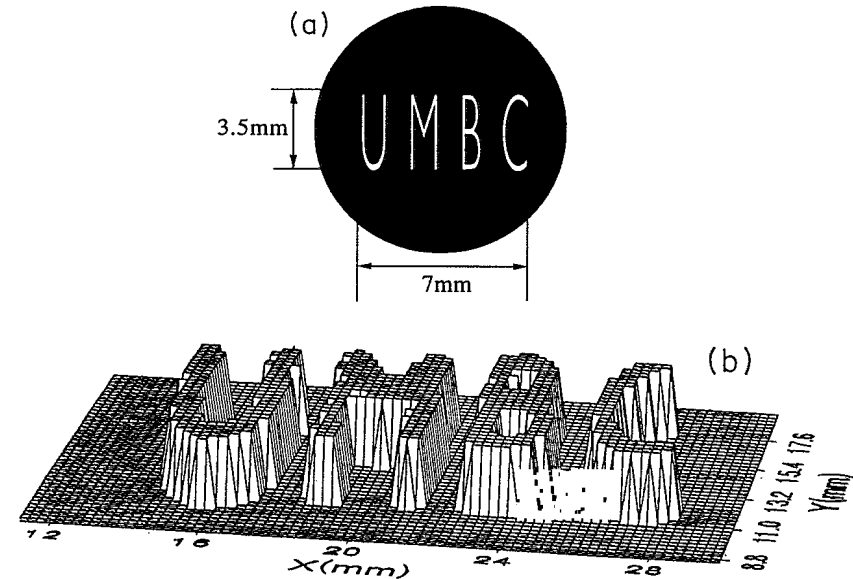
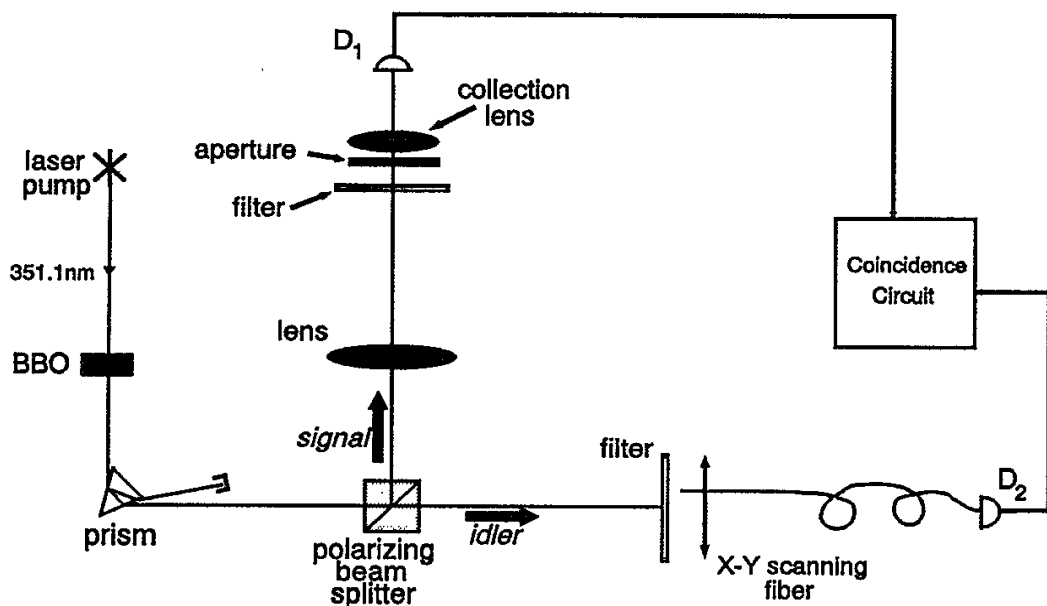
NOVEMBER 1995

Optical imaging by means of two-photon quantum entanglement

T. B. Pittman, Y. H. Shih, D. V. Strekalov, and A. V. Sergienko

Department of Physics, University of Maryland Baltimore County, Baltimore, Maryland 21228

(Received 22 December 1994)



Ghost imaging history

PRL 94, 063601 (2005)

PHYSICAL REVIEW LETTERS

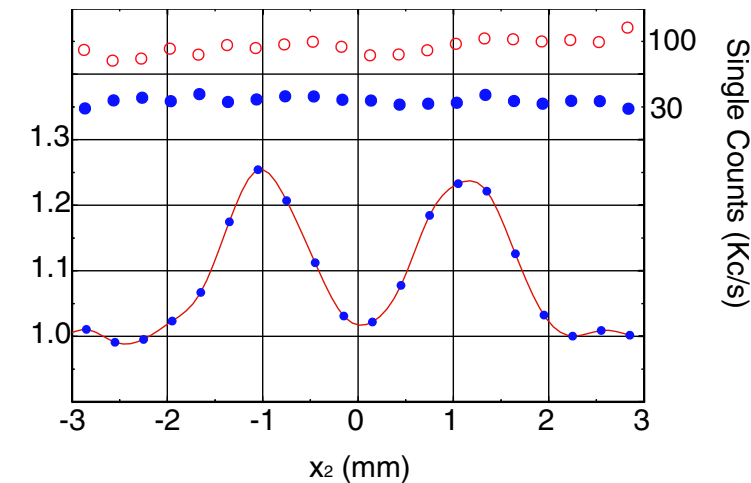
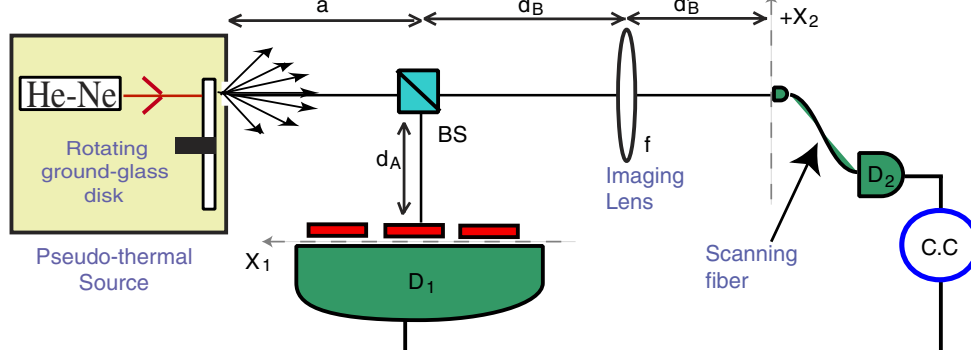
week ending
18 FEBRUARY 2005

Two-Photon Imaging with Thermal Light

Alejandra Valencia, Giuliano Scarcelli, Milena D'Angelo, and Yanhua Shih

Department of Physics, University of Maryland, Baltimore County, Baltimore, Maryland 21250, USA

(Received 30 July 2004; published 16 February 2005)



Ghost imaging history

PRL 94, 183602 (2005)

PHYSICAL REVIEW LETTERS

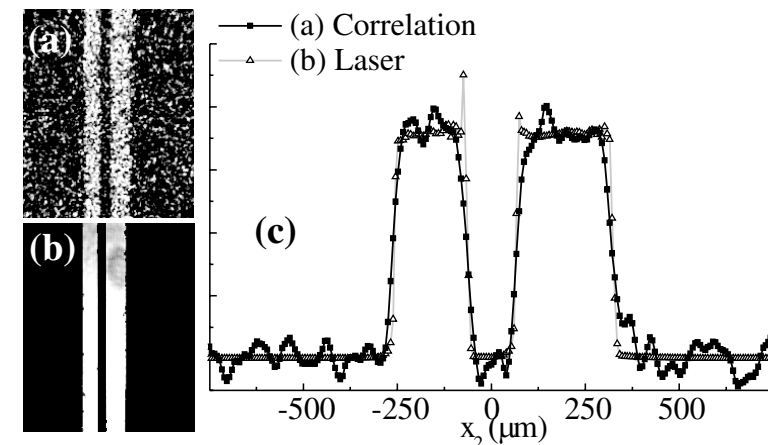
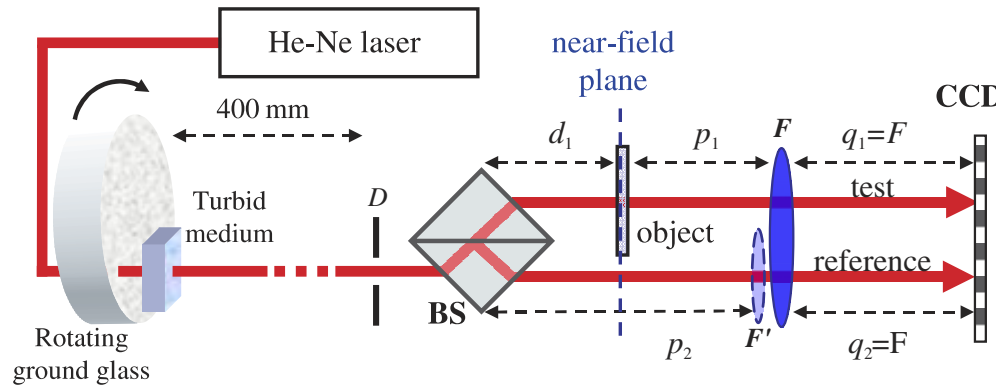
week ending
13 MAY 2005

High-Resolution Ghost Image and Ghost Diffraction Experiments with Thermal Light

F. Ferri, D. Magatti, A. Gatti, M. Bache, E. Brambilla, and L. A. Lugiato

INFN, Dipartimento di Fisica e Matematica, Università dell'Insubria, Via Valleggio 11, 22100 Como, Italy

(Received 2 September 2004; published 12 May 2005)



Ghost imaging history

VOLUME 93, NUMBER 9

PHYSICAL REVIEW LETTERS

week ending
27 AUGUST 2004

Ghost Imaging with Thermal Light: Comparing Entanglement and Classical Correlation

A. Gatti, E. Brambilla, M. Bache, and L. A. Lugiato

INFM, Dipartimento di Fisica e Matematica, Università dell'Insubria, Via Valleggio 11, 22100 Como, Italy

(Received 25 July 2003; published 26 August 2004)

We consider a scheme for coherent imaging that exploits the classical correlation of two beams obtained by splitting incoherent thermal radiation. This case is analyzed in parallel with the configuration based on two entangled beams produced by parametric down-conversion, and a precise formal analogy is pointed out. This analogy opens the possibility of using classical beams from thermal radiation for ghost imaging schemes in the same way as entangled beams.

DOI: 10.1103/PhysRevLett.93.093602

PACS numbers: 42.50.-p, 42.50.Dv, 42.50.Ar

Ghost imaging history

Unified Theory of Ghost Imaging with Gaussian-State Light

Baris I. Erkmen* and Jeffrey H. Shapiro

Massachusetts Institute of Technology, Research Laboratory of Electronics, Cambridge, Massachusetts 02139, USA

(Dated: February 2, 2008)

The theory of ghost imaging is developed in a Gaussian-state framework that both encompasses prior work—on thermal-state and biphoton-state imagers—and provides a complete understanding of the boundary between classical and quantum behavior in such systems. The core of this analysis is the expression derived for the photocurrent-correlation image obtained using a general Gaussian-state source. This image is expressed in terms of the phase-insensitive and phase-sensitive cross-correlations between the two detected fields, plus a background. Because any pair of cross-correlations is obtainable with classical Gaussian states, the image does not carry a quantum signa-

Erkmen and Shapiro showed

1. Ghost imaging is not unique to quantum light sources
2. **Phase-sensitive ghost imaging** can also be implemented classically

Phase-sensitive vs. Phase-insensitive

Phase-insensitive ghost imaging

Has only phase-insensitive cross-correlations

Far-field image signature is upright

One Fresnel number: $D_0 = k_0 \rho_0 a_0 / 2L$

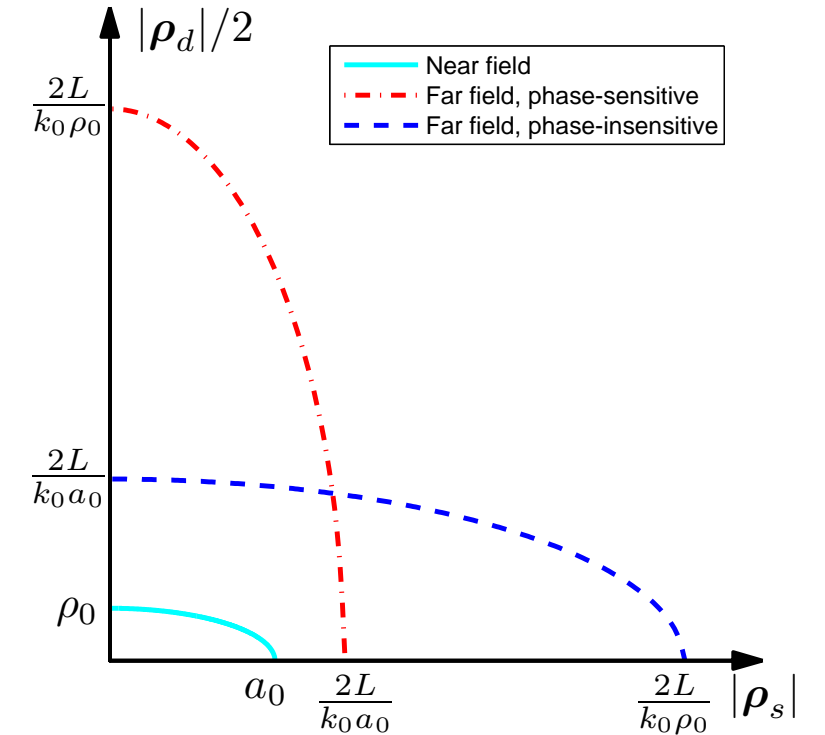
Phase-sensitive ghost-imaging

Has only phase-sensitive cross-correlations

Far-field image signature is inverted

Two Fresnel numbers: $D_F = k_0 \rho_0^2 / 2L$

$$D_N = k_0 a_0^2 / 2L$$



$$K_{S,R}^{(x)}(\rho_1, \rho_2) = \frac{2P}{\pi a_0^2} e^{-(|\rho_1|^2 + |\rho_2|^2)/a_0^2 - |\rho_2 - \rho_1|^2/2\rho_0^2}$$

Another classical phase-sensitive source

In PC-OCT, we implemented a classical phase-sensitive light source using **amplified SPDC**

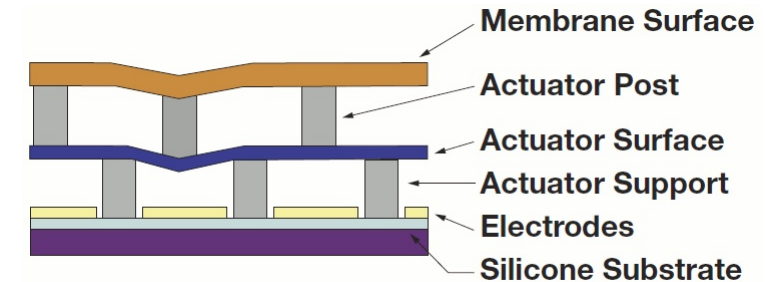
For GI we use **a pair of spatial-light modulators** (SLMs) driven with deterministic, anti-correlated pseudorandom phases



SLM principles of operation

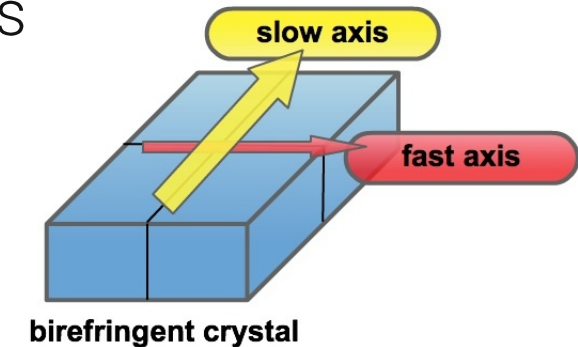
Mechanically-driven SLMs translate individual pixels using PZT or MEMS

- » Pros: high-speed modulation (10-100 kHz)
- » Cons: pixel cross-talk, expensive
- » Polarization-independent

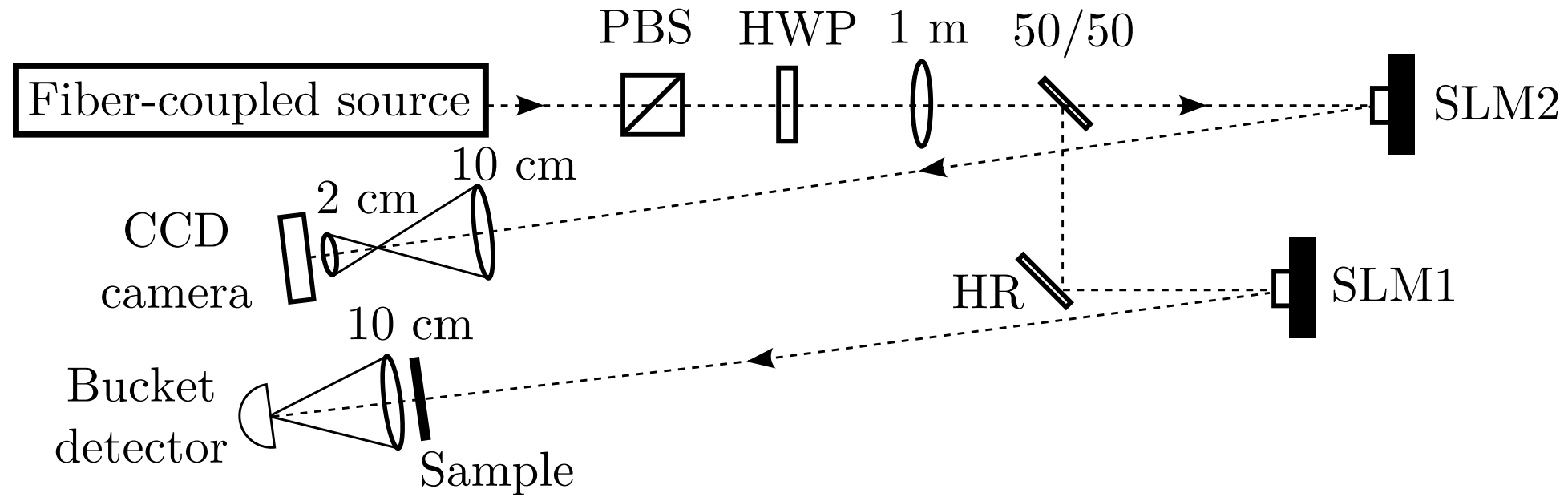


Liquid-crystal SLMs use electric field and birefringent crystals

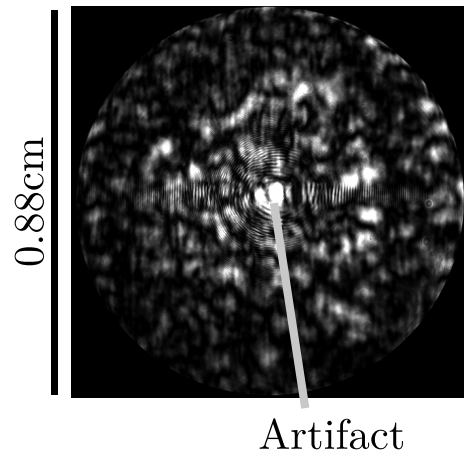
- » Pros: low cross-talk, convertible to intensity modulator
- » Cons: slow (~1-100 Hz), calibration issues, dead region
- » Polarization-dependent



Experimental setup

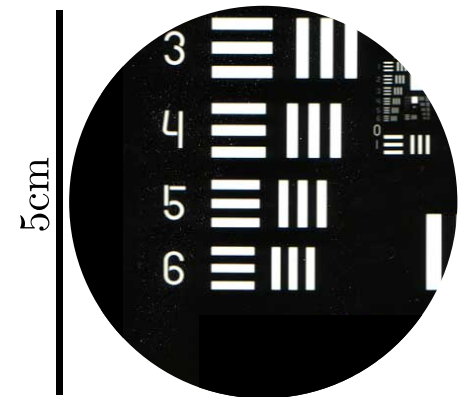


Results



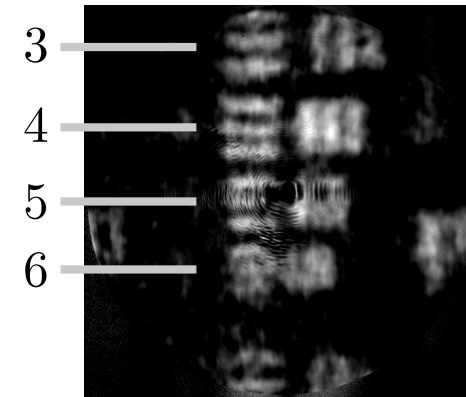
0.88cm

Artifact

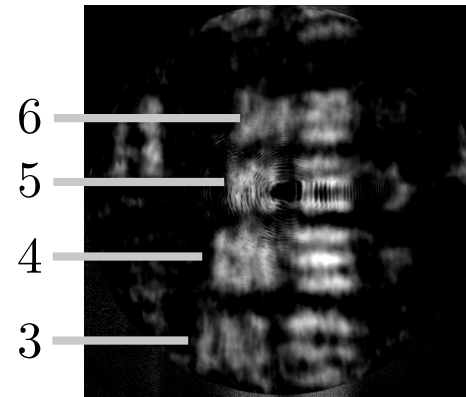


Sample speckle pattern as seen by CCD

USAF resolution test transmission mask

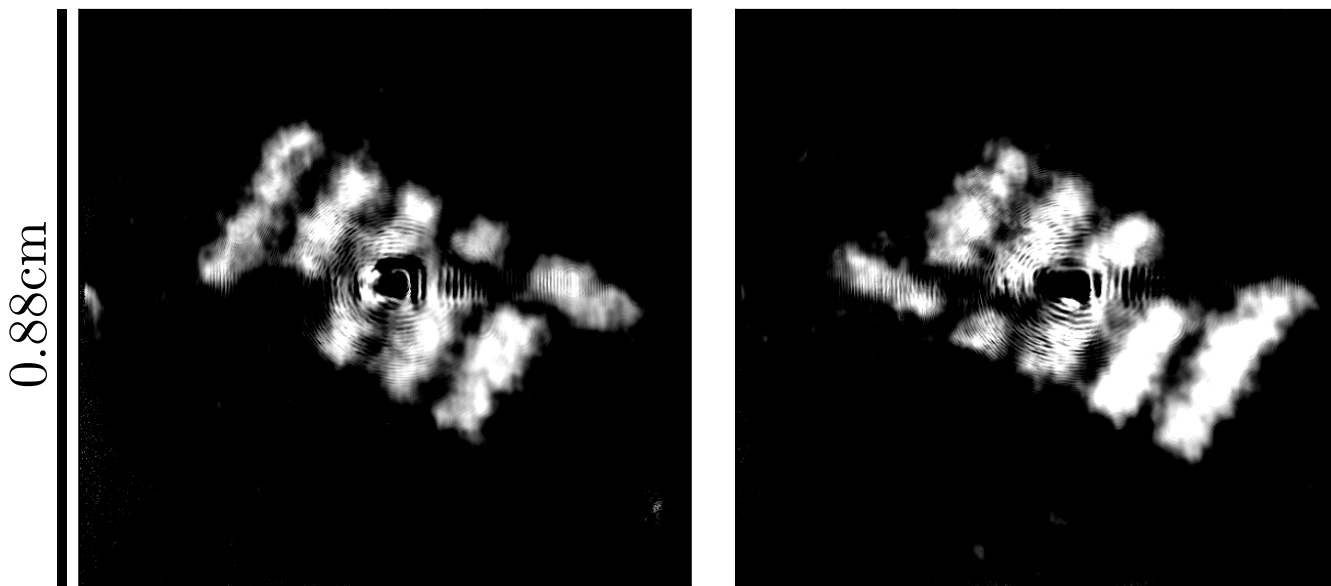


Phase-insensitive ghost imaging result (upright)



Phase-sensitive ghost imaging result (inverted)

Results

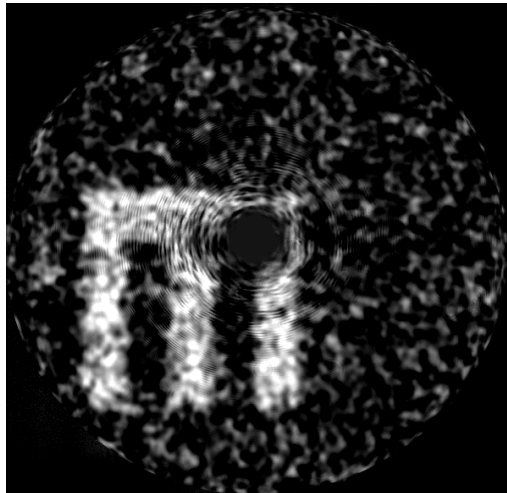


Phase-insensitive

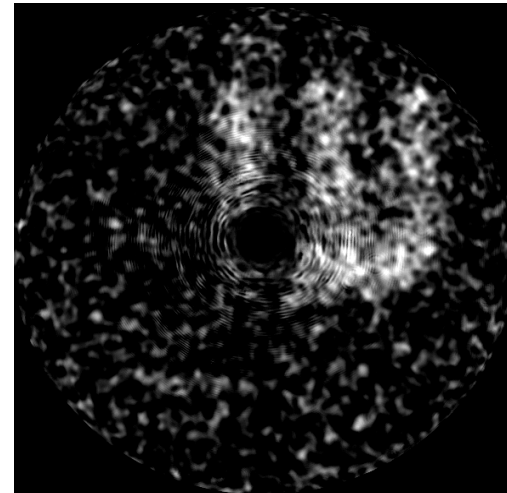
Phase-sensitive

Results

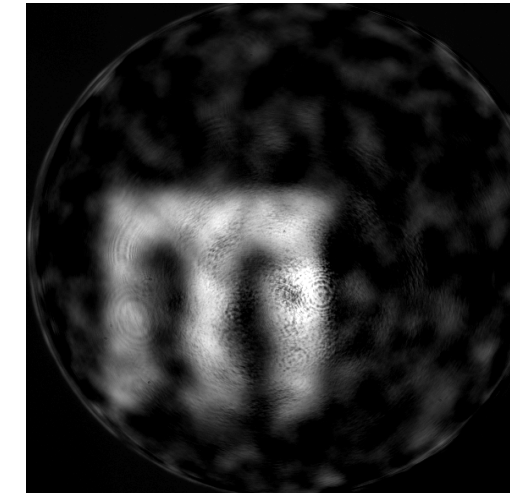
Phase-sensitive operation highly sensitive to focusing parameters if SLMs not located at beam waist ($2.75 z_R$ in this case)



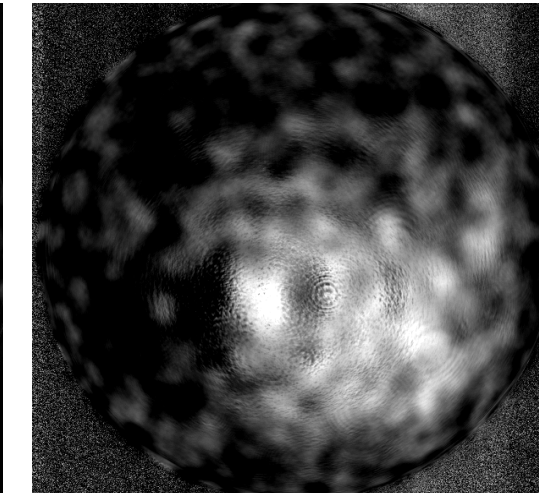
Phase-insensitive



Phase-sensitive



Phase-insensitive



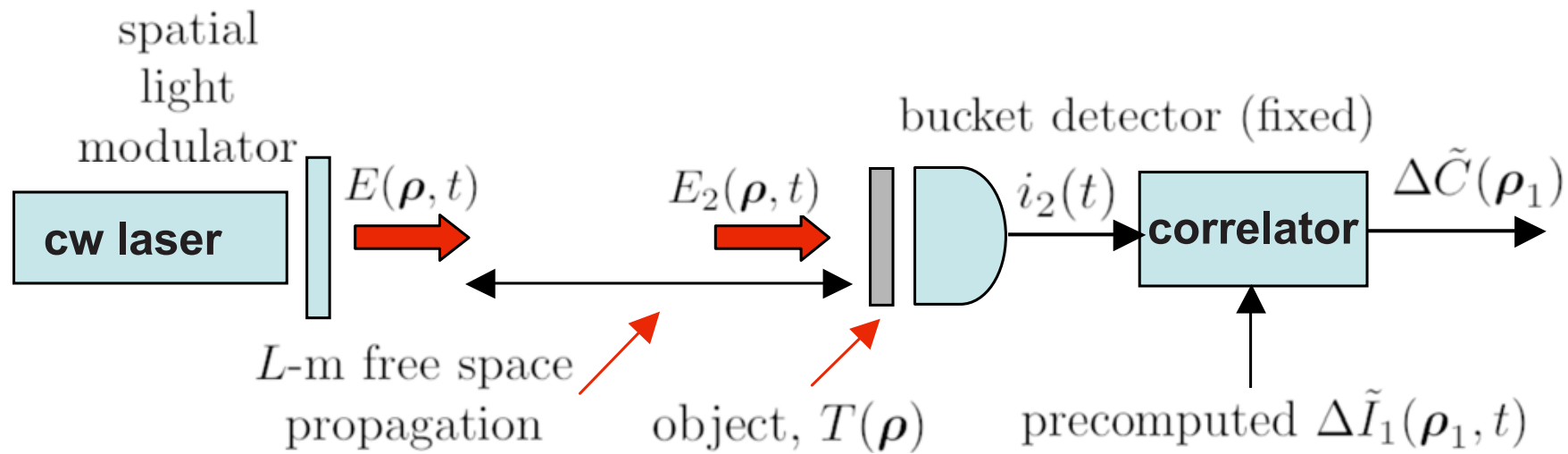
Phase-sensitive

Loose focusing

Tight focusing

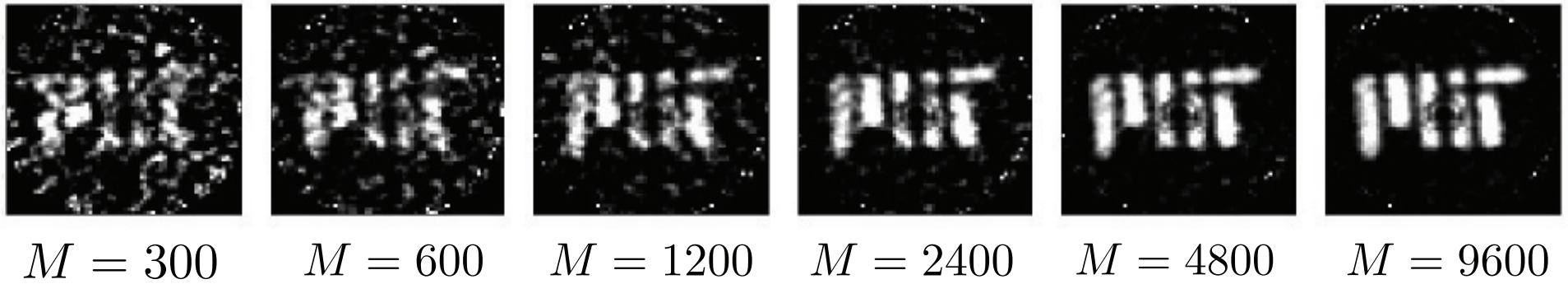
Computational ghost imaging

Since both signal and reference arm phase patterns are deterministic, we can replace the reference arm with a simulation

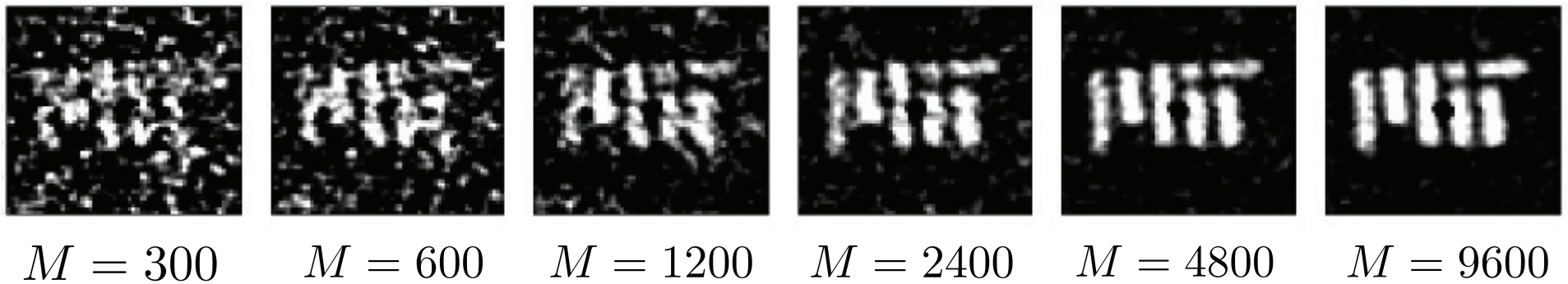


Computational ghost imaging

Physical



Simulated

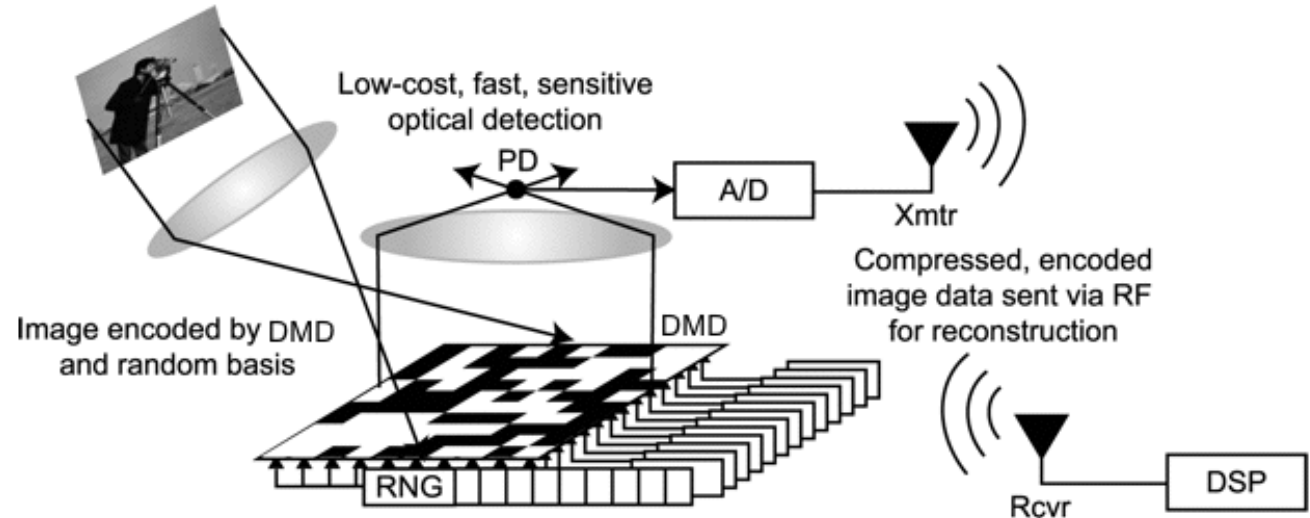


Compressive ghost imaging

Averaging to obtain image is slow

GI similar to Rice University single-pixel camera

Exploit spatial structure (sparsity) to recover object from a small set of data by computational optimization



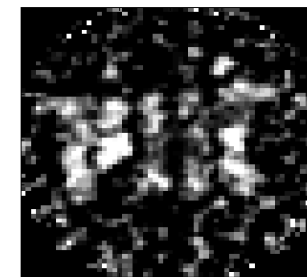
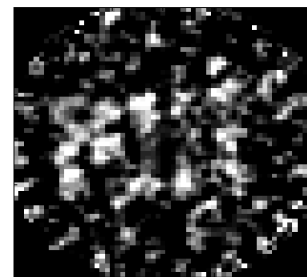
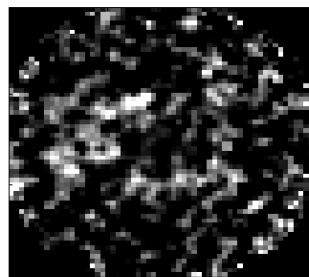
M.F. Duarte, et al. Signal Processing Magazine, IEEE, 25(2):83–91, March 2008.

$$\hat{x} = \arg \min_x \|W\{x\}\|_1, \text{ s. t. } \|Ax - b\|_2 < \epsilon$$

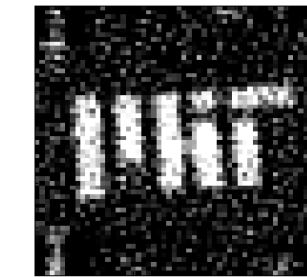
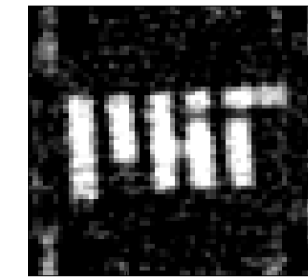
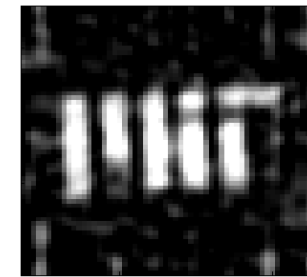
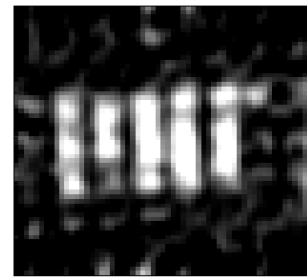
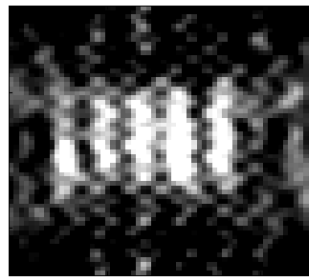
Compressive ghost imaging

Factor of ~ 10 speedup by using compressive sensing in DCT basis

BS + CCD GI



BS + CCD GI
(L1 min DCT)



M=100

M=200

M=400

M=800

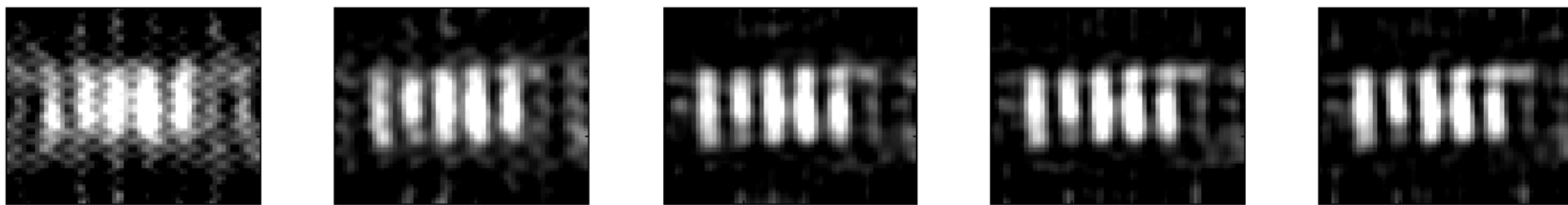
M=1200

M=4800

Compressive ghost imaging

Total variation instead of DCT gives even faster results for binary masks

(a) DCT



(b) TV



100

200

400

600

800

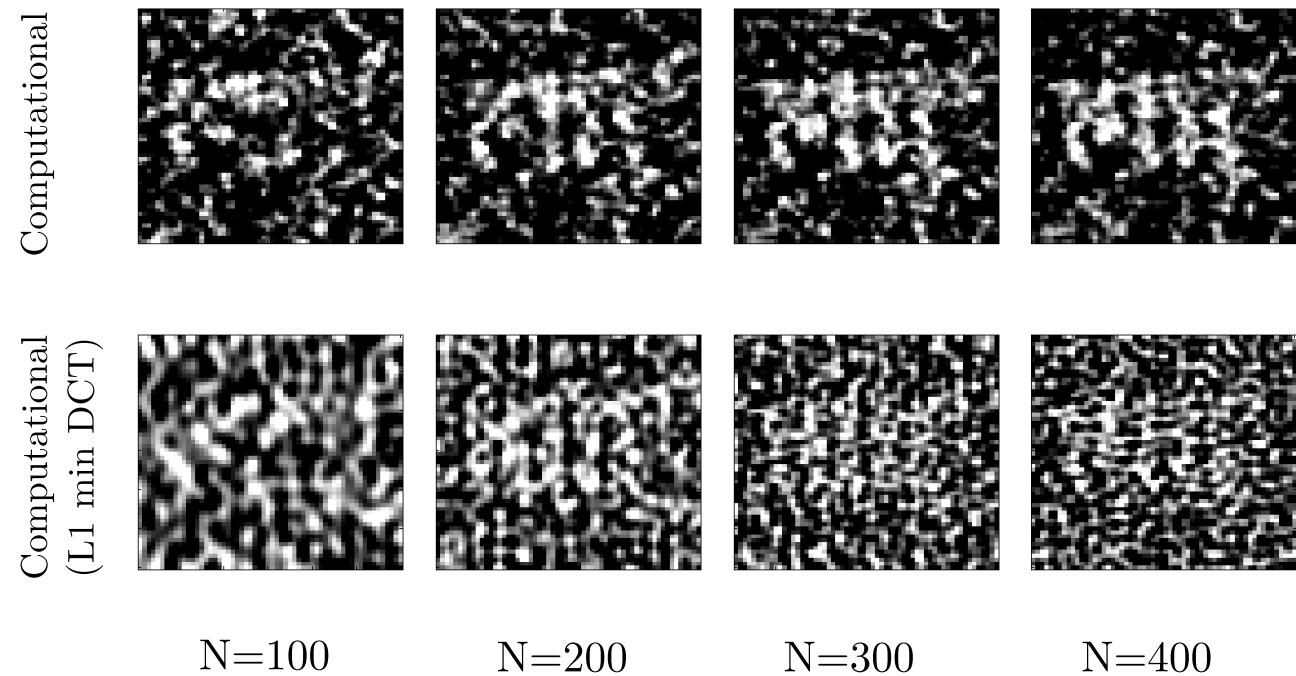
Number of realizations

Computational compressive GI

Does not work as expected

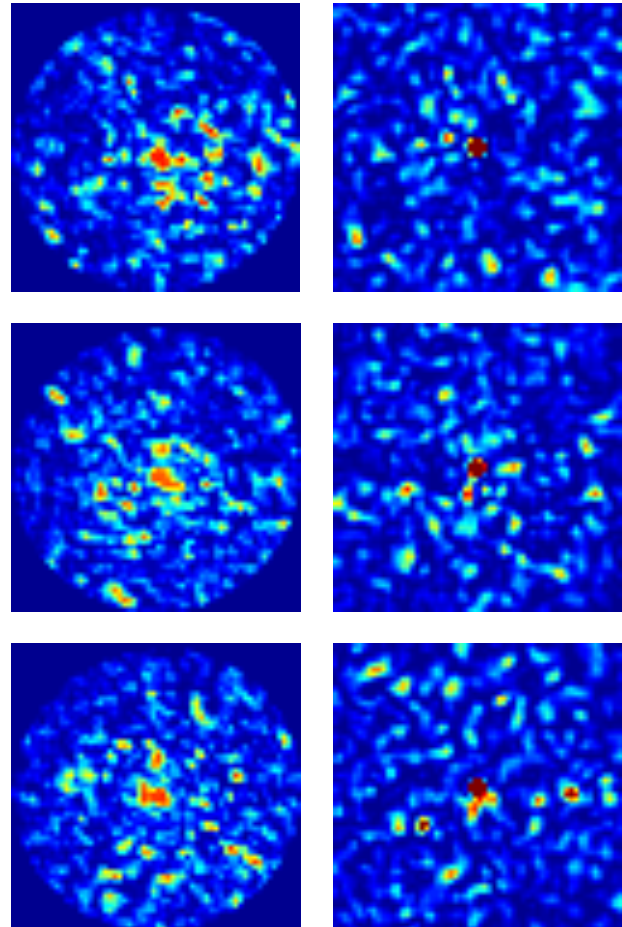
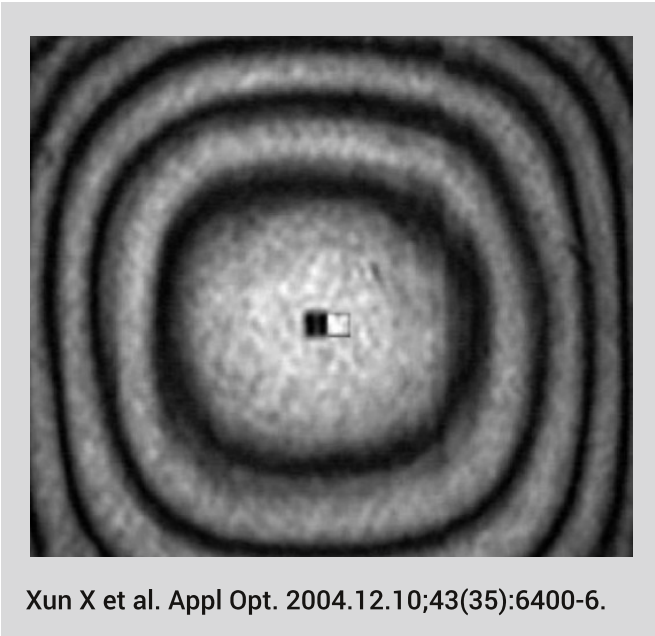
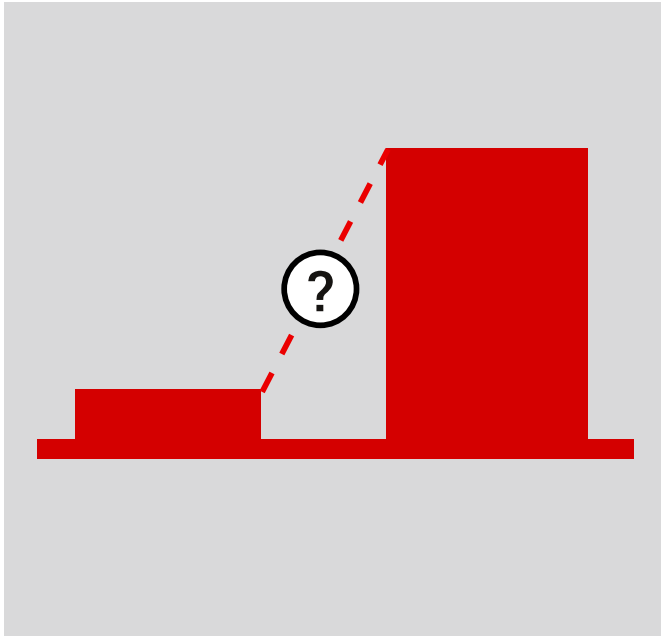
SLM imperfections: dead-space behavior, flatness, calibration

In **compressive GI** we used a beamsplitter so did to see effects of these imperfections



In **computational GI** we averaged out the imperfections over thousands of realizations

SLM imperfections



Dead-space behavior

May have cross-talk
with active pixels

SLM not flat

Several-wavelength
deviations

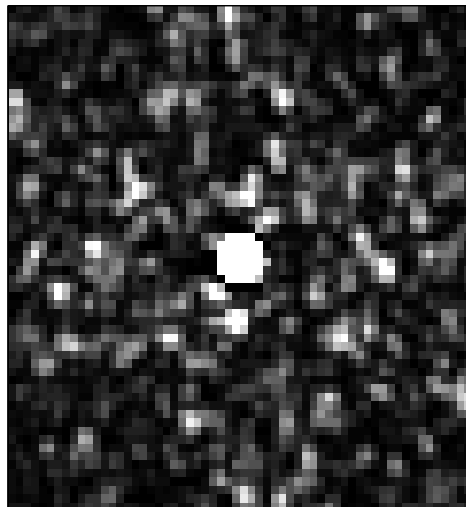
CCD image

Simulation

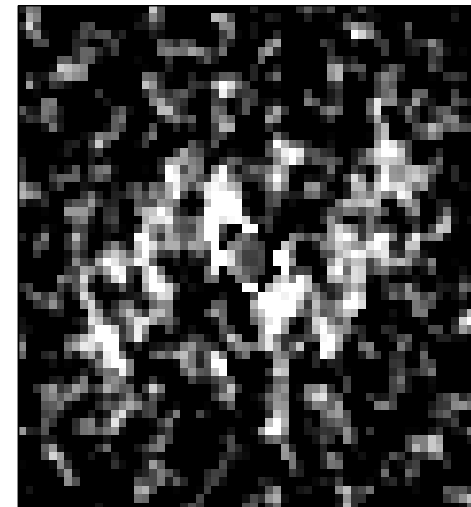
Computational compressive GI

Need more predictable SLM for far-field ghost imaging

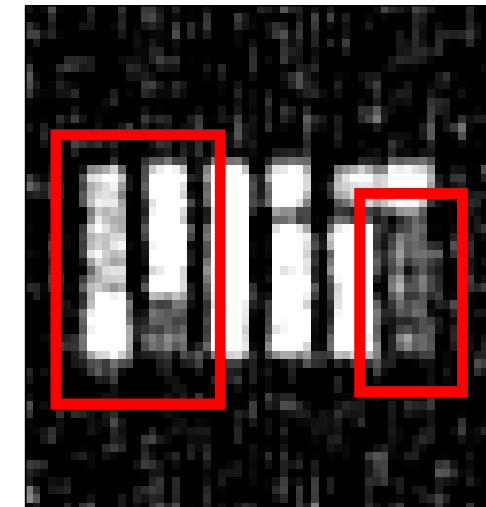
Digital micromirror devices more predictable, but since they only modulate reflectivity and not phase, they are only suitable for near-field operation



Sample speckle



Averaging ($M=500$)



CS ($M=500$)

DMD simulation results show phase-sensitive (inverted) and phase-insensitive (upright) images superimposed

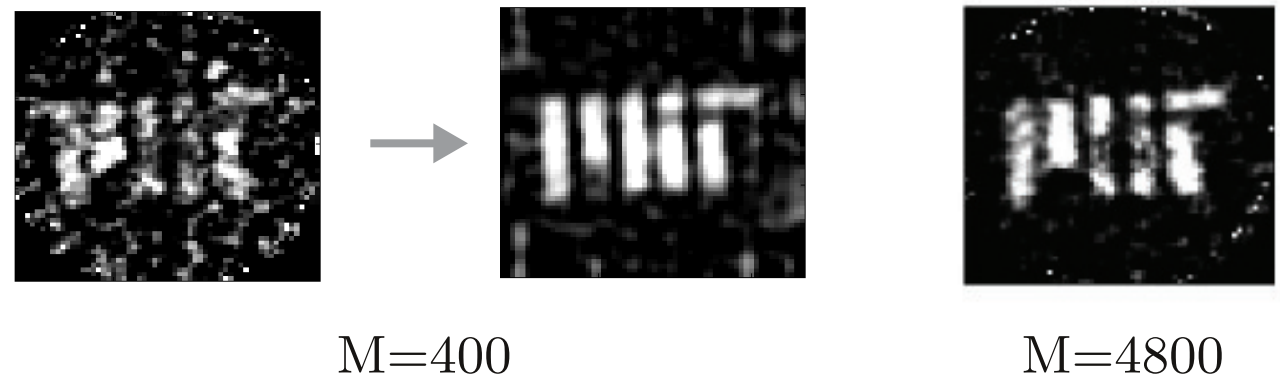
CS helps but still shows artifacts

4 EXPERIMENT

Single-photon imaging

Motivation

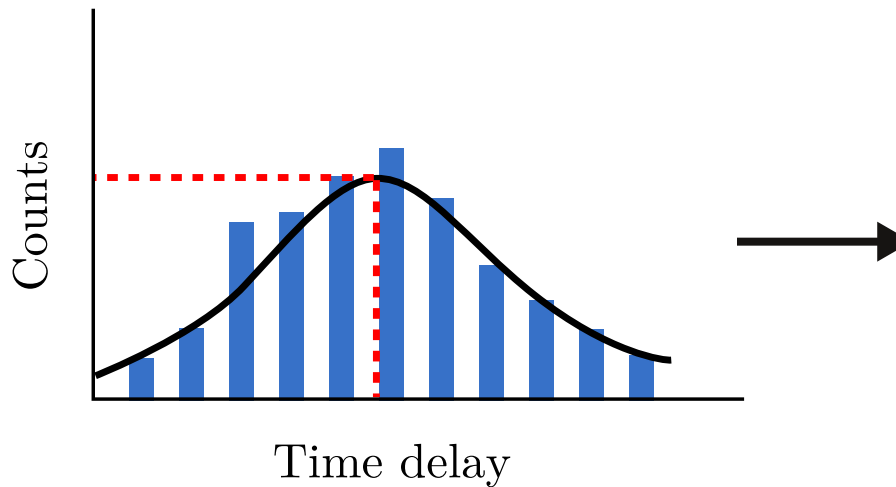
In ghost imaging, we used computational reconstruction to recover a clean image using a small number of measurements



Can we use this for depth and reflectivity imaging in a more general sense?

Traditional active imaging

Use pulsed, periodic illumination and histogram **tens to hundreds of photons per pixel** of data to obtain accurate depth and reflectivity maps



One-pixel histogram



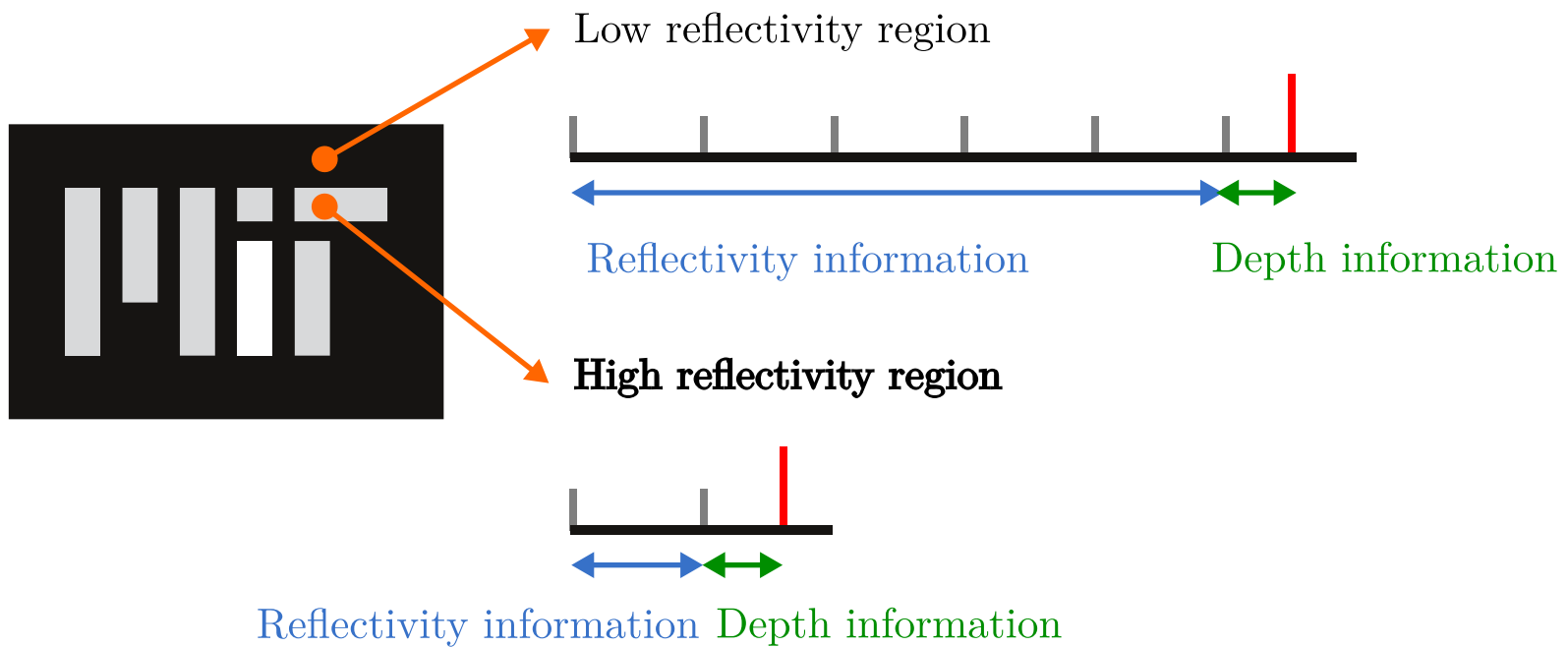
Reflectivity map



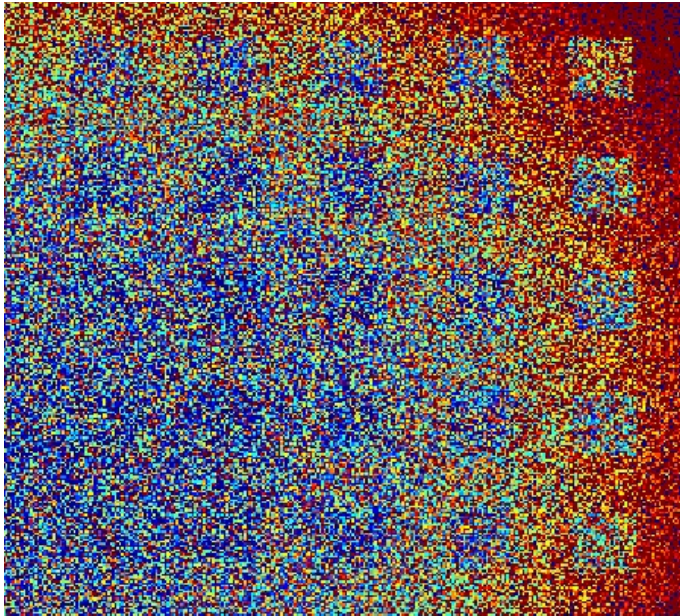
Depth map

First-photon imaging

What if we only used **1 photon per pixel**?



First-photon imaging



Problem:

Poor-quality images, corrupted by pulse width (depth) and Poisson noise (reflectivity)



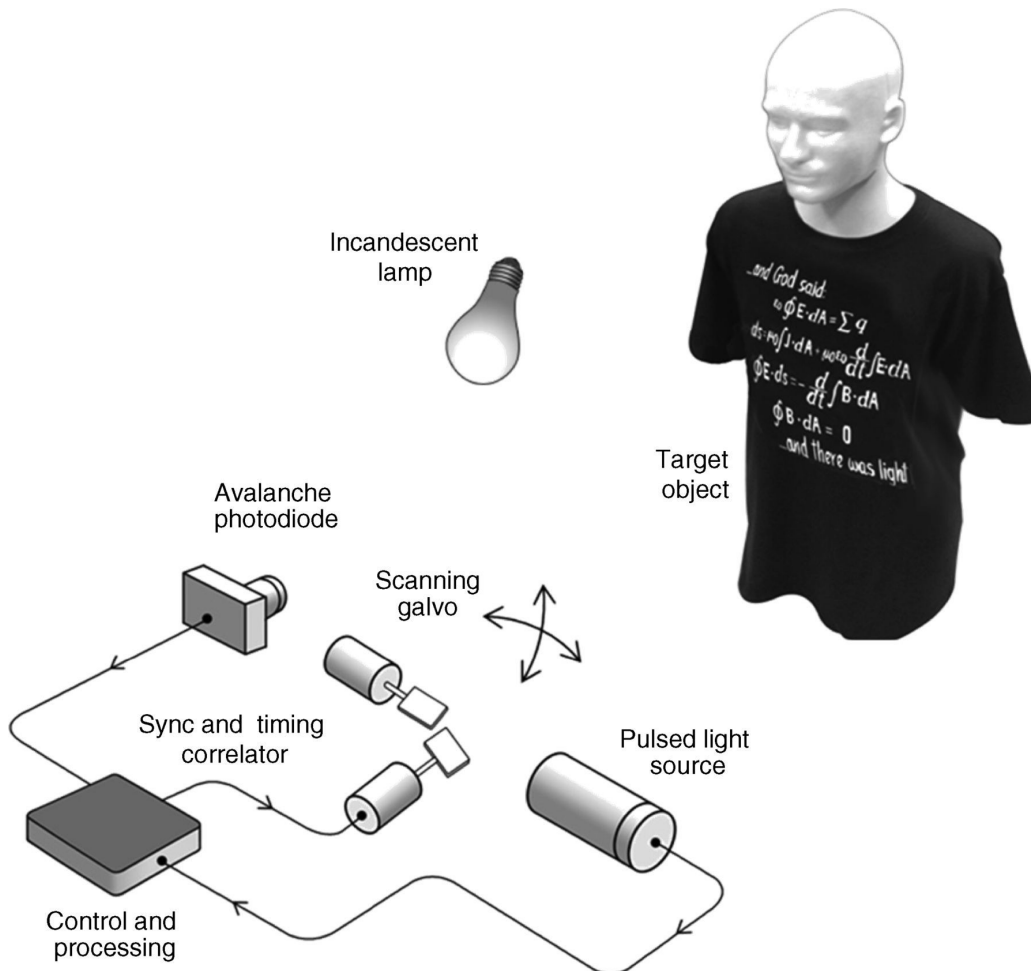
Solution:

Use knowledge of single-photon detection statistics

Similar to compressive GI, assume object is realistic and has spatial correlations

Use computational optimization to reconstruct the scene given a small amount of data (1 photon per pixel)

Experimental setup



Illumination:

Laser: 640-nm, 10 MHz repetition rate,
226-ps RMS width

Raster scanning:

2-axis galvo mirror: $\pm 20^\circ$, 1000×1000 scan

Detection:

APD: 100×100 μm , 50-ps jitter, 35% efficiency
IF: 2-nm bandwidth, 49% transmission
TDC: 8-ps resolution

Computational reconstruction algorithm

Step 1: Reflectivity reconstruction

Minimize a weighted sum of the log-likelihood given Poisson statistics and a sparsity-promoting term:

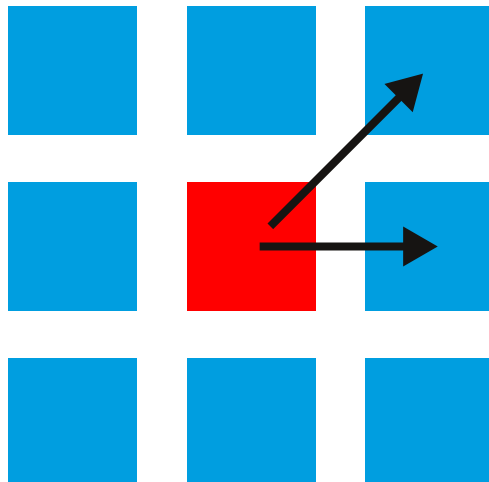
$$\{\hat{\alpha}(x, y)\} = \arg \min_{\{\alpha(x, y)\}} (1 - \beta) \left[\sum_x \sum_y \mathcal{L}(\alpha(x, y) | n(x, y)) \right] + \beta \|\Phi(\{\alpha(x, y)\})\|_1$$

$$\mathcal{L}(\alpha(x, y) | n(x, y)) = \gamma [\alpha(x, y)S + BT_r] [n(x, y) - 1] - \log [\gamma \alpha(x, y)S + BT_r]$$

Computational reconstruction algorithm

Step 2: Background noise censoring

Background noise makes depth reconstruction non-convex. We eliminate background photons using the ROAD statistic:

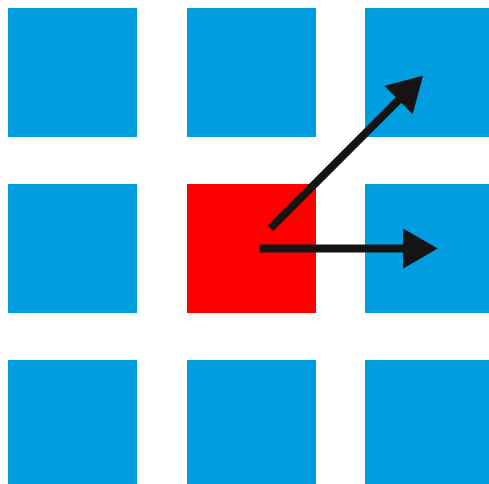


1. Calculate differences to nearest 8 pixels $|t(x_1, y_1) - t(x, y)|, \dots, |t(x_8, y_8) - t(x, y)|$
2. Sort in ascending order
3. Define $\text{ROAD}(x, y)$ to be the sum of the first 4 values

Computational reconstruction algorithm

Step 2: Background noise censoring

Background noise makes depth reconstruction non-convex. We eliminate background photons using the ROAD statistic:



4. Binary decision test: If $\text{ROAD}(x, y) > C$, reject pixel and replace with average of neighboring 8 pixels.

$$C = 4T_p \frac{BT_r}{\hat{\alpha}(x, y)S + BT_r}$$

Computational reconstruction algorithm

Step 3: Depth reconstruction

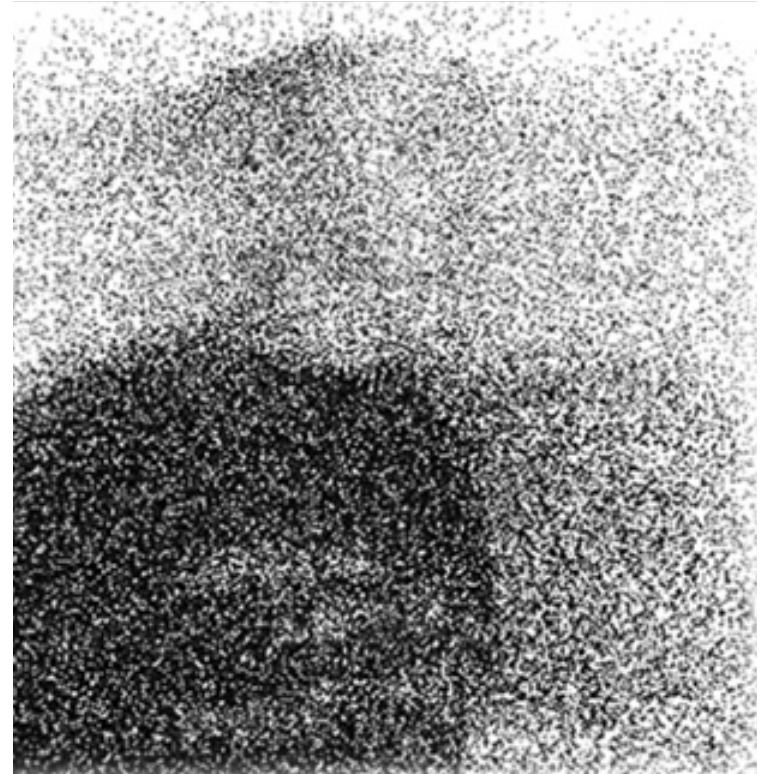
Minimize a weighted sum of the log-likelihood given pulse shape and a sparsity-promoting term:

$$\{\hat{Z}(x, y)\} = \arg \min_{\{Z(x, y)\}} (1 - \beta) \left[\sum_x \sum_y \mathcal{L}(Z(x, y) | t(x, y)) \right] + \beta \|\Phi(\{Z(x, y)\})\|_1$$

$$\mathcal{L}(Z(x, y) | t(x, y)) = -\log \left[s(t(x, y) - \frac{2Z(x, y)}{c}) \right]$$

Results

Raw ML estimates



Results

Reflectivity reconstruction



Results

Background noise censoring

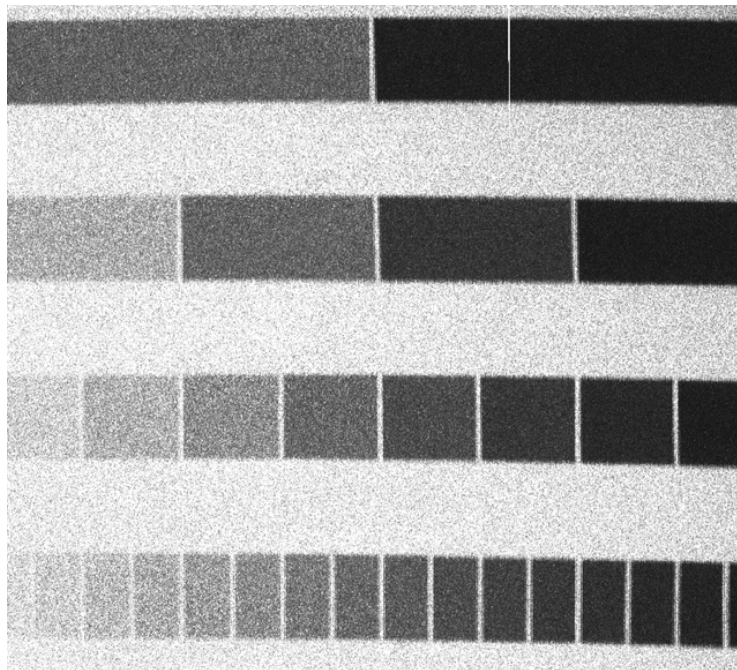


Results

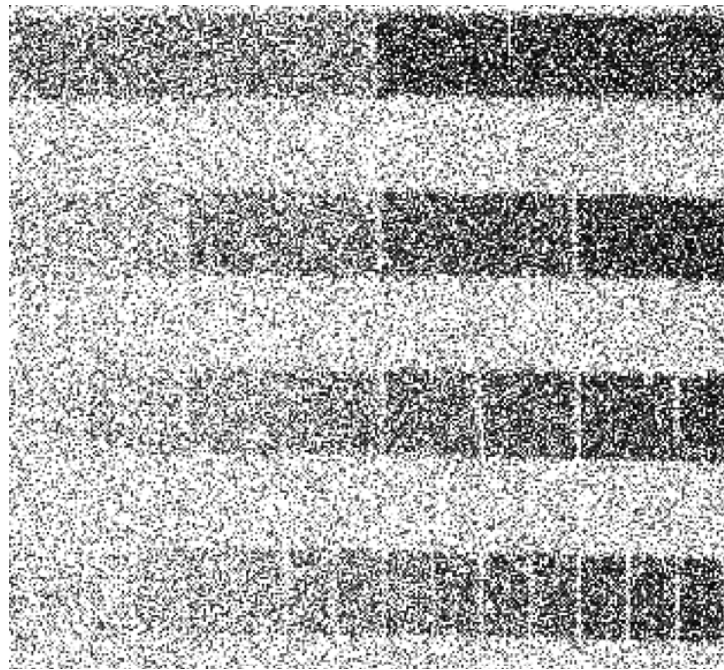
Depth reconstruction



Results: Reflectivity chart



Reference measurement
(~1000 photos/pixel)

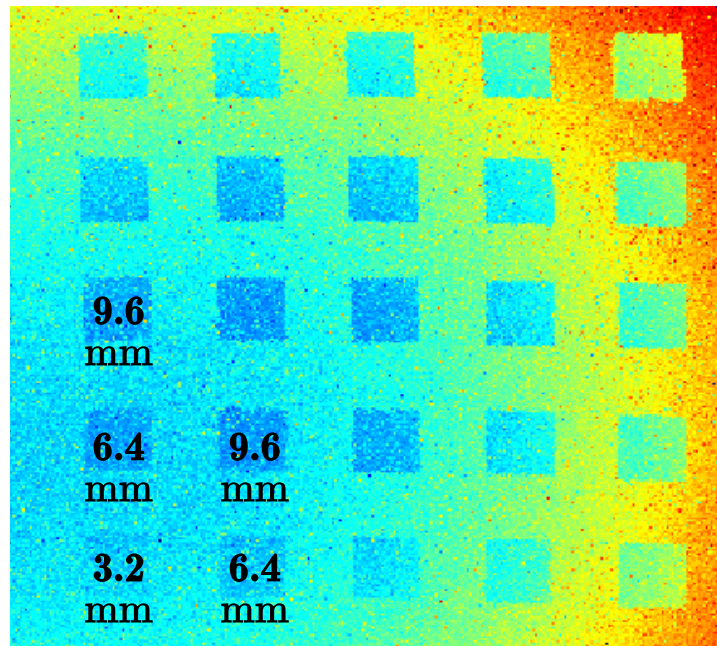


First-photon ML estimate

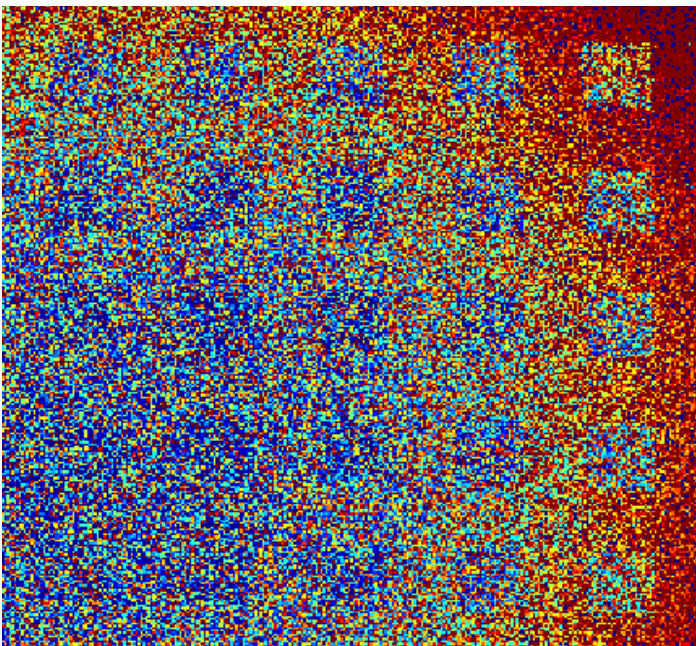


First-photon, reconstructed

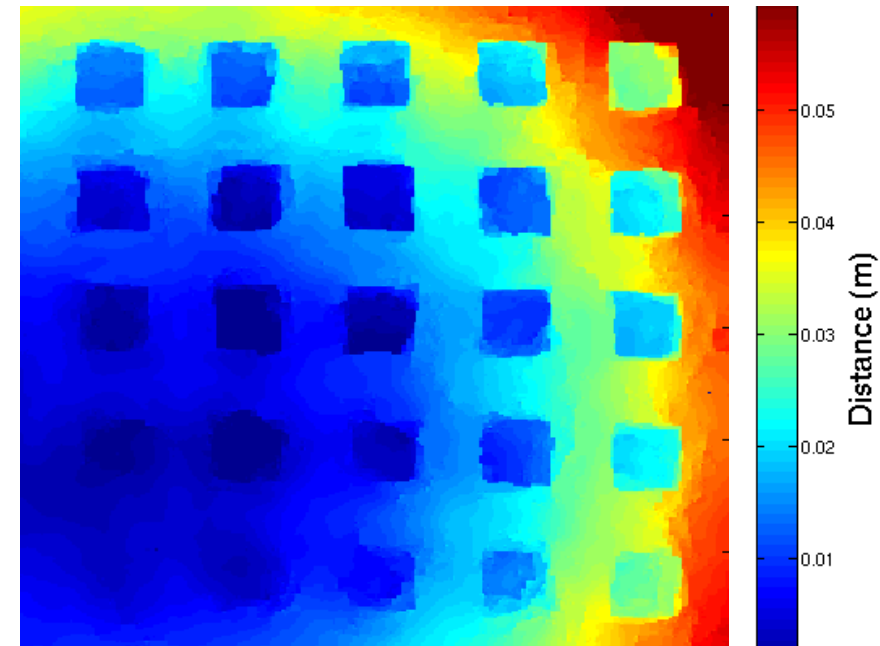
Results: Depth chart



Reference measurement
(~1000 photos/pixel)



First-photon ML estimate



First-photon, reconstructed

SPAD array imaging

Established research collaboration with
Zappa group, Politecnico di Milano

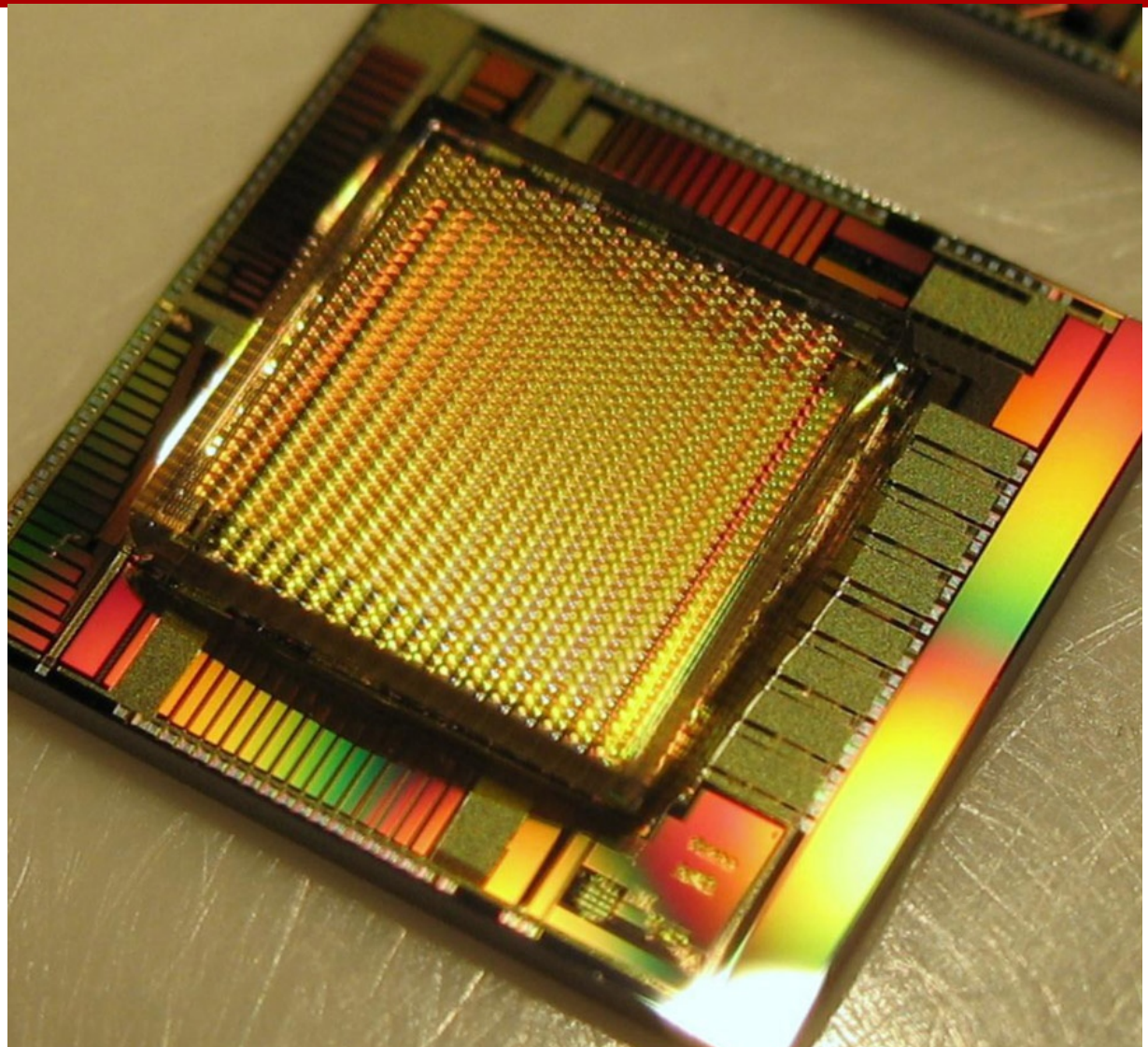
Borrowed prototype of a 32×32 pixel
SPAD array with 6-bit TDC at each pixel

Counting mode:

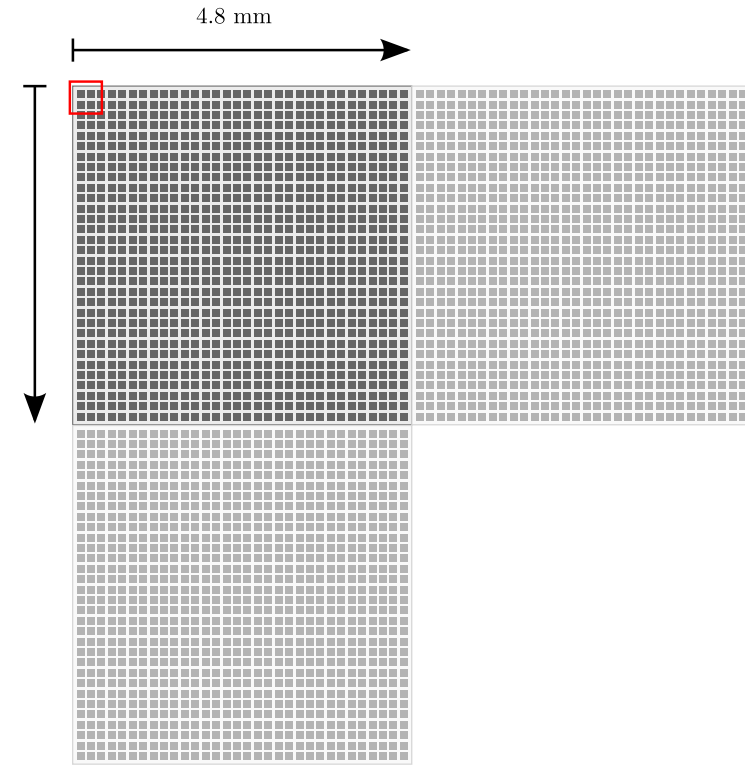
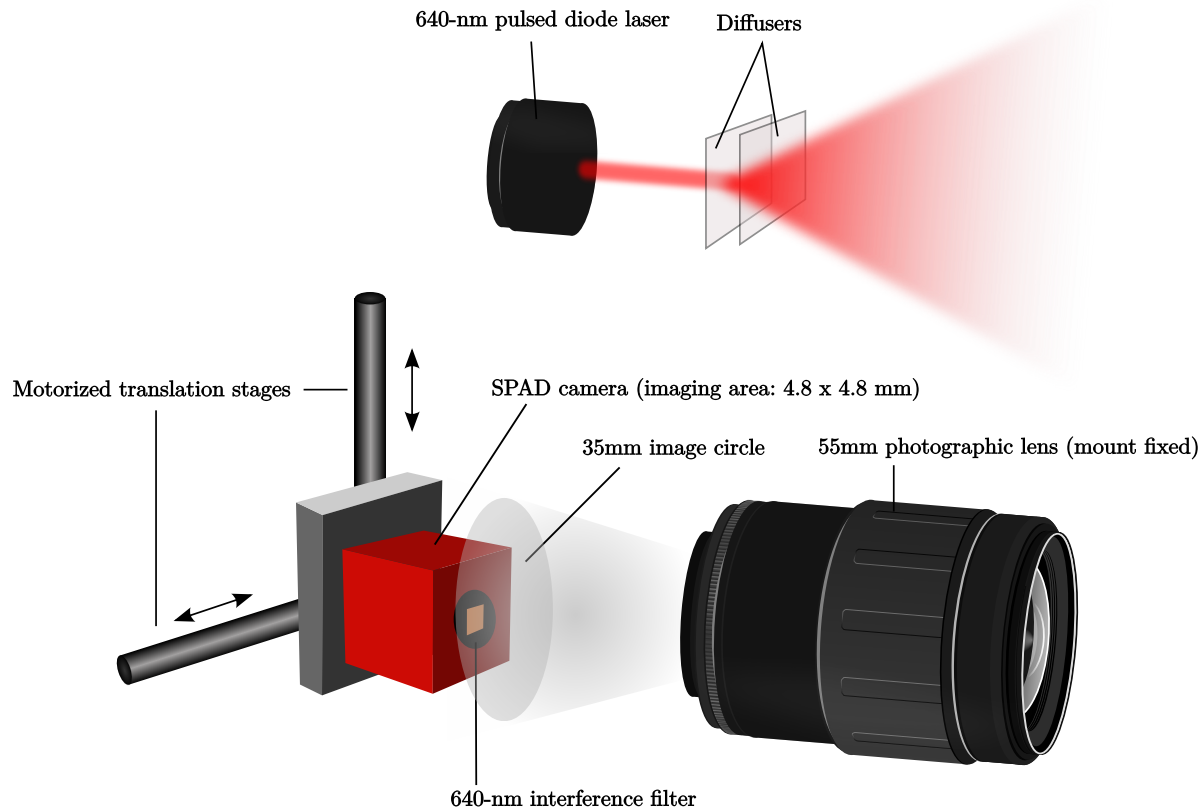
6-bit resolution (0-63 photon arrivals)

Timing mode:

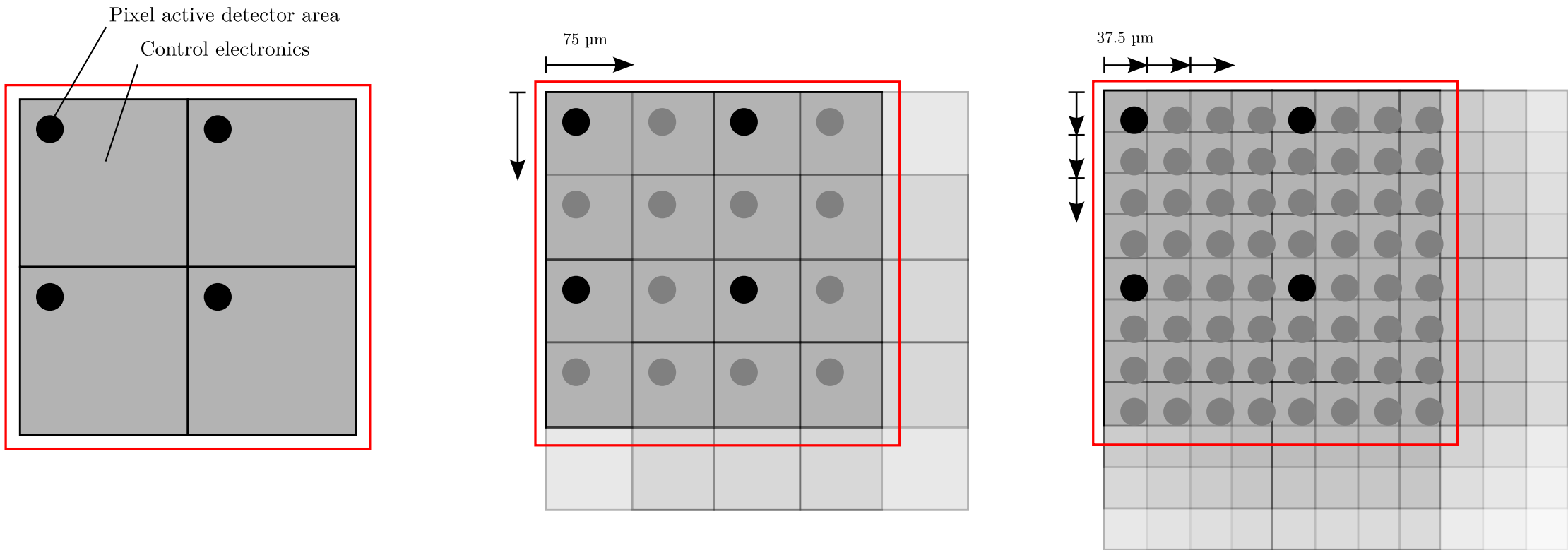
10-bit, 1024 bins, each 389.9 ps



SPAD array imaging



Subpixel scanning for higher resolution



Computational reconstruction algorithm

Step 1: Reflectivity reconstruction

Instead of time until first arrival, we now use the number of photon detection events in a fixed dwell period.

$$\mathcal{L}(\alpha(x, y) | n(x, y)) = \gamma [\alpha(x, y)S + BT_r] [n(x, y) - 1] - \log [\gamma\alpha(x, y)S + BT_r]$$



$$\mathcal{L}(\alpha(x, y) | k(x, y)) = \gamma [\alpha(x, y)S + BT_r] [N - k(x, y)] - k(x, y) \log [1 - \exp [-\gamma\alpha(x, y)S + BT_r]]$$

Computational reconstruction algorithm

Step 2: Background noise censoring

1. Compute $t_{ROM}(x, y)$ = median value of all detections in neighboring 8 pixels
2. Define a set of indices of detections to keep as valid, rejecting the others.

$$U(x, y) = \left\{ \ell : |t_\ell(x, y) - t_{ROM}(x, y)| < 2T_p \left(\frac{BT_r}{\gamma\alpha(x, y)S + BT_r} \right), 0 \leq \ell < k(x, y) \right\}$$

Computational reconstruction algorithm

Step 3: Depth reconstruction

Instead of using only first arrival, we make use of all valid data.

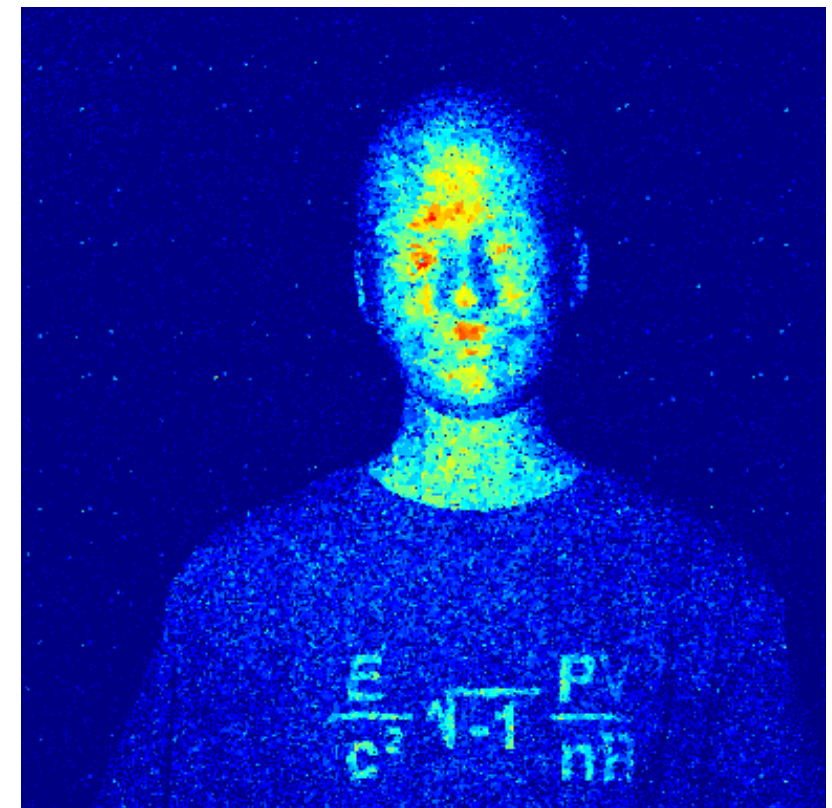
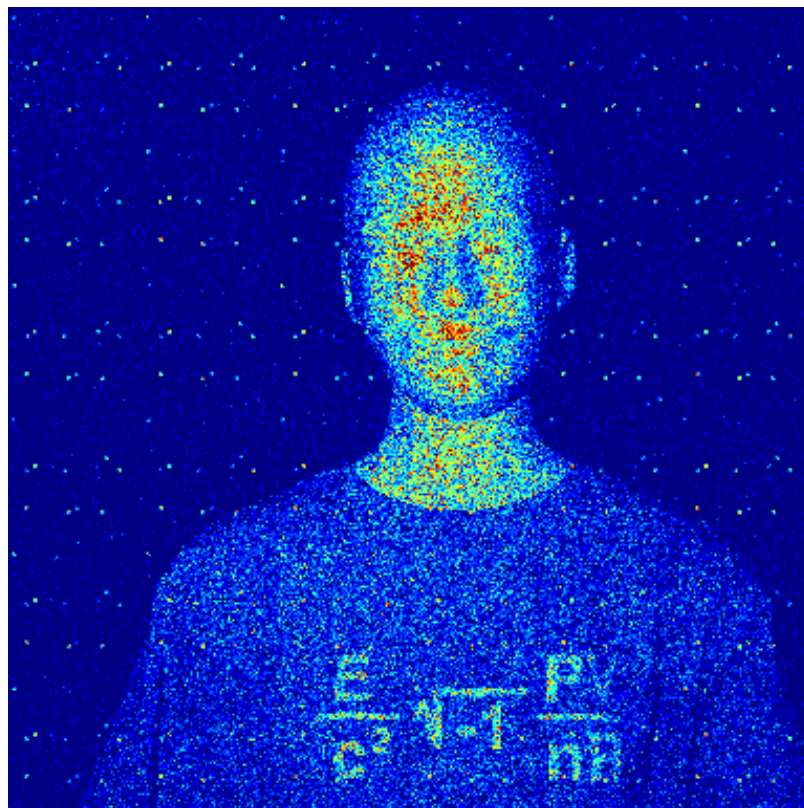
$$\mathcal{L}(Z(x,y)|t(x,y)) = -\log \left[s(t(x,y) - \frac{2Z(x,y)}{c}) \right]$$



$$\mathcal{L}(Z(x,y)|\{t_\ell(x,y)|\ell \in U(x,y)\}) = -\sum_{\ell \in U(x,y)} \log \left[s(t_\ell(x,y) - \frac{2Z(x,y)}{c}) \right]$$

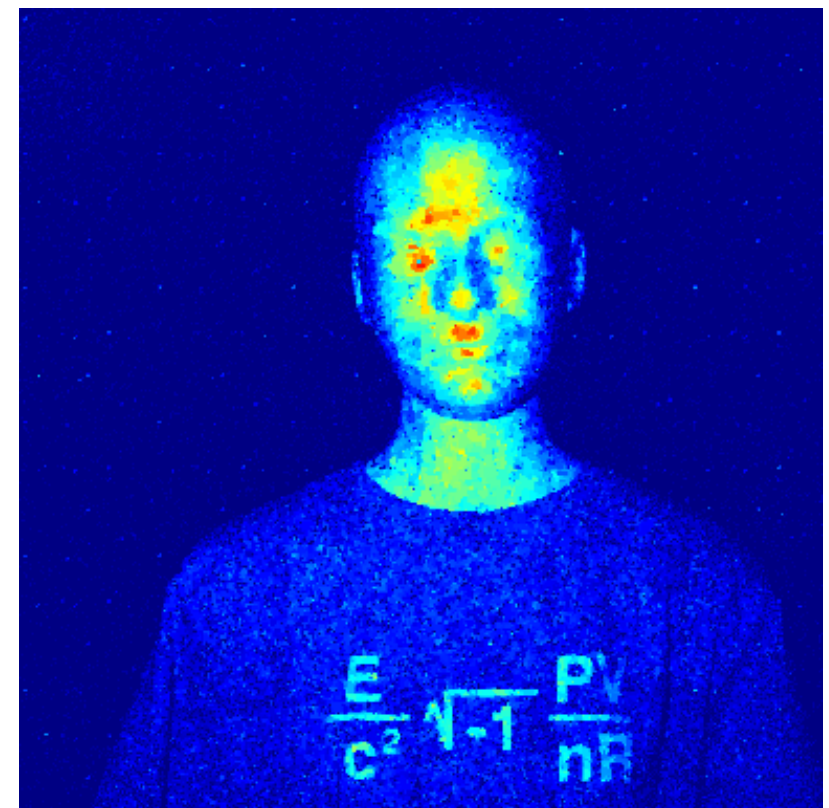
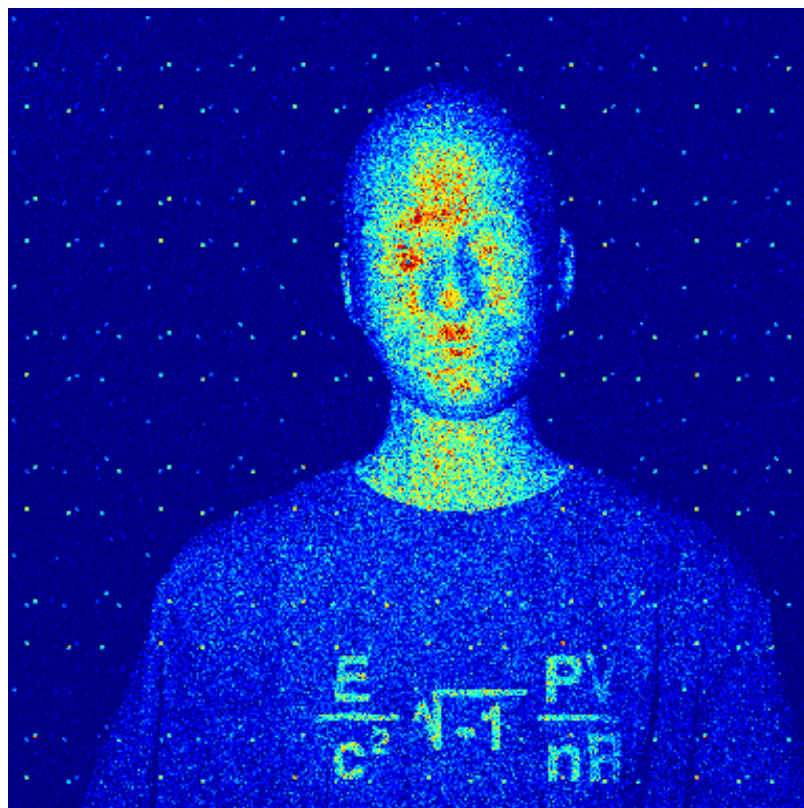
Results: Reflectivity

25 frames



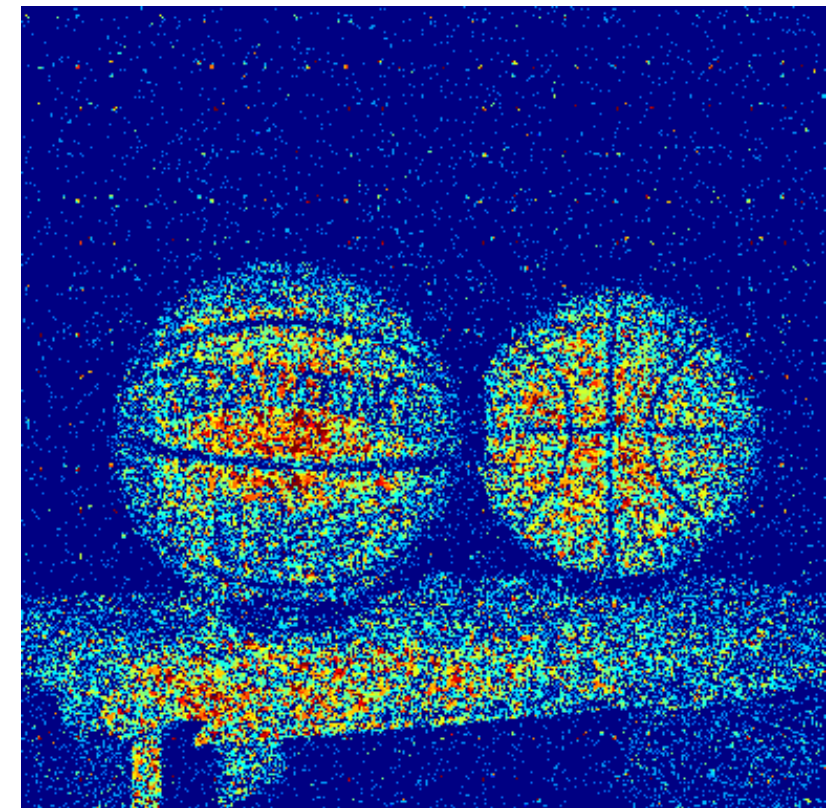
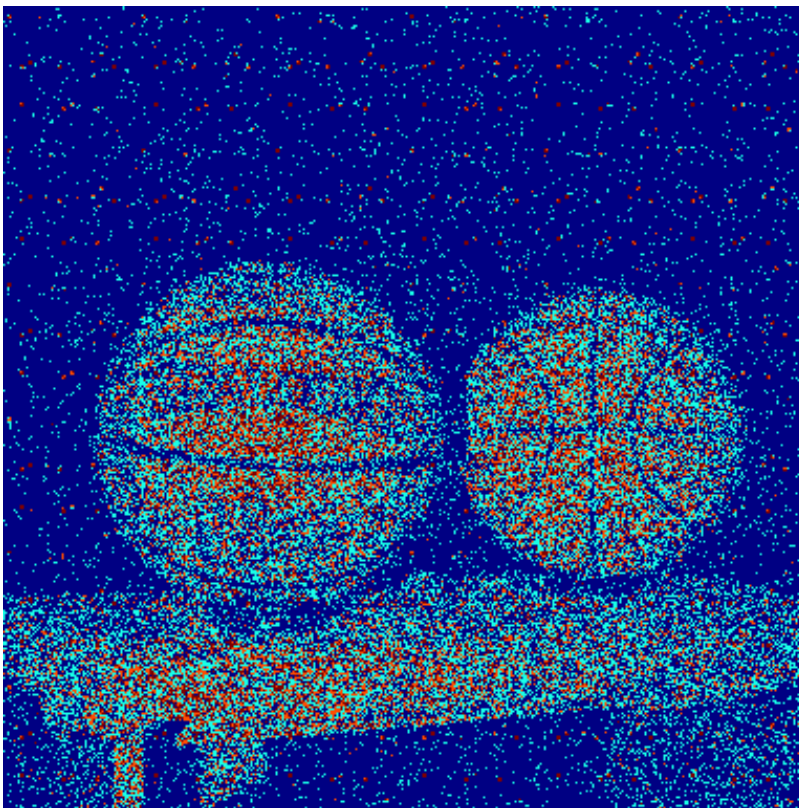
Results: Reflectivity

50 frames



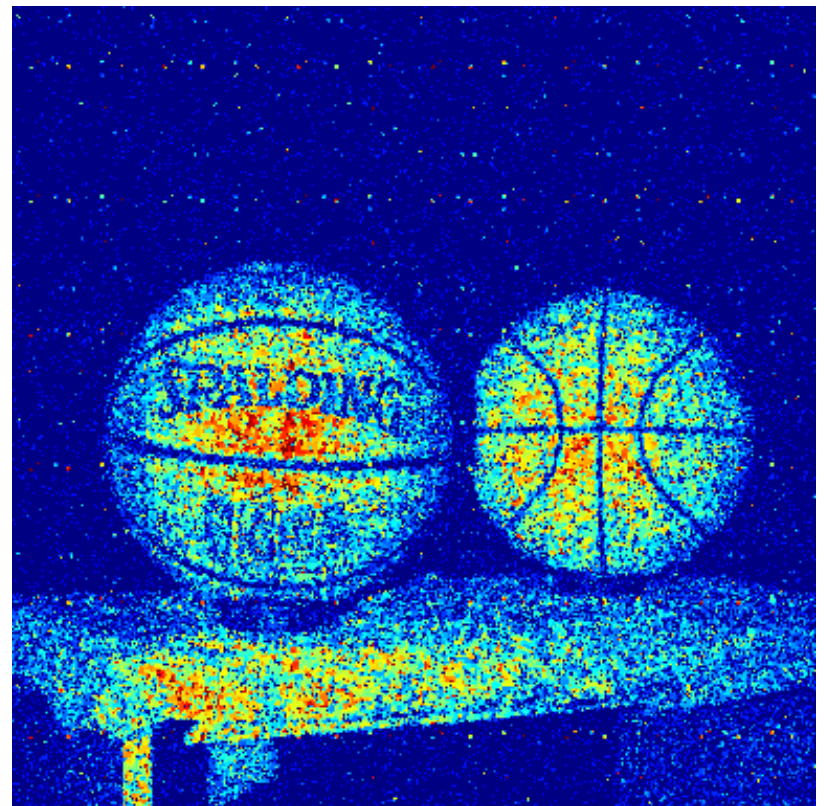
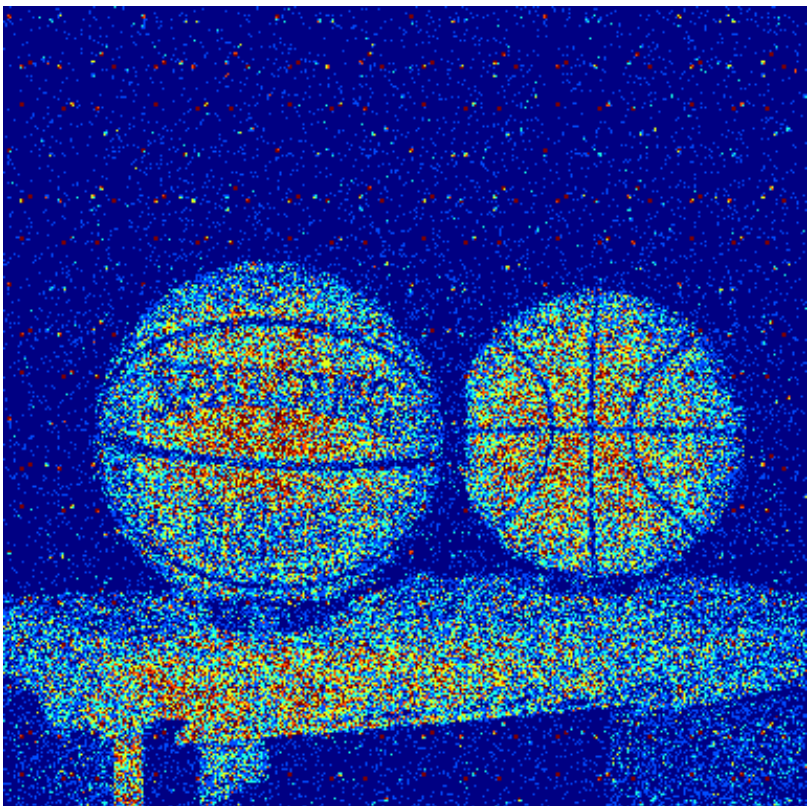
Results: Reflectivity

25 frames



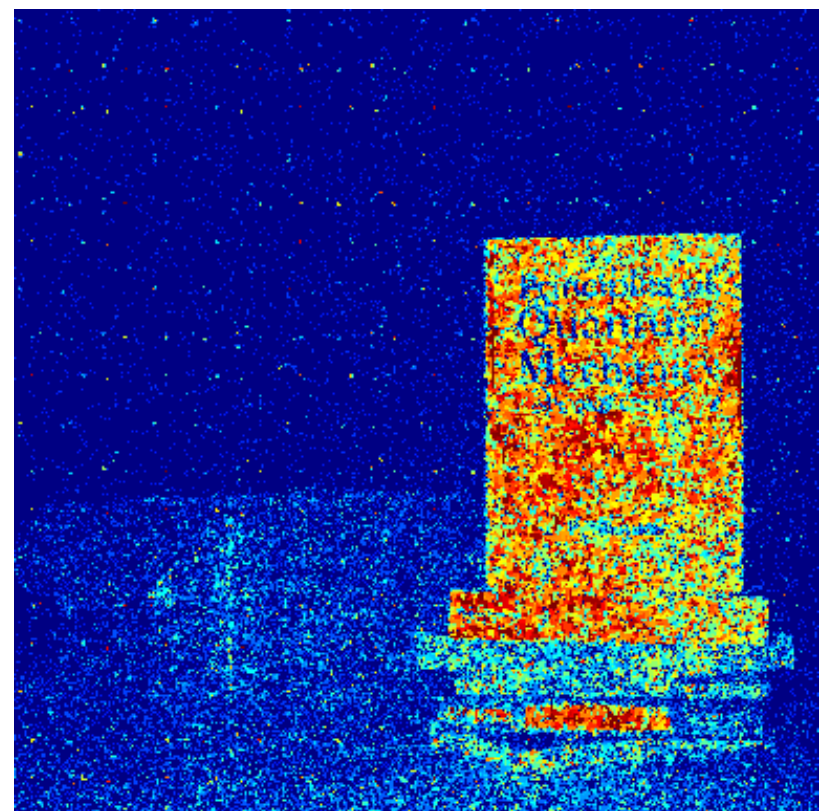
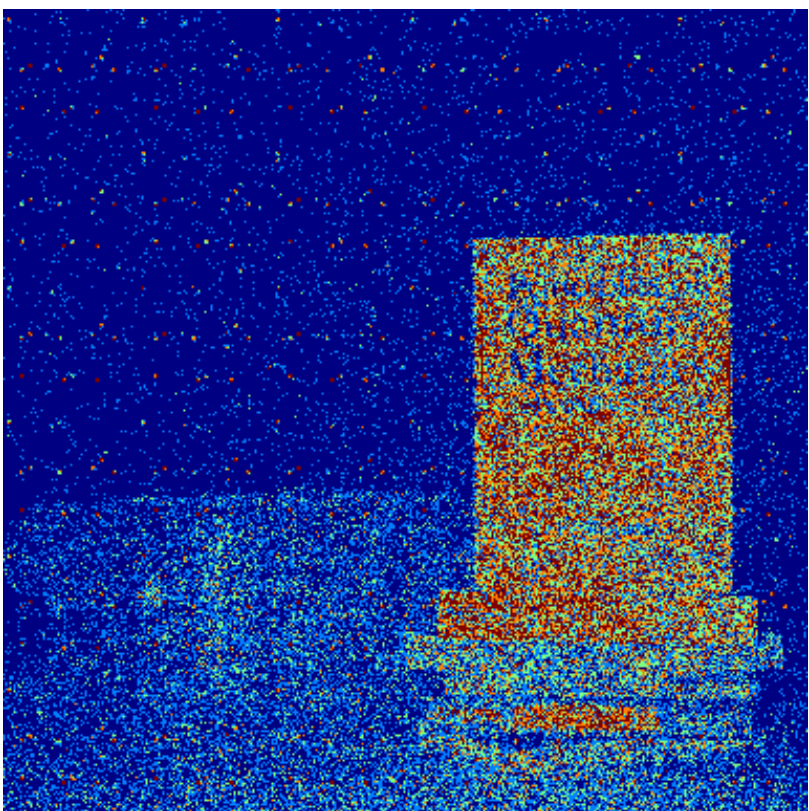
Results: Reflectivity

50 frames



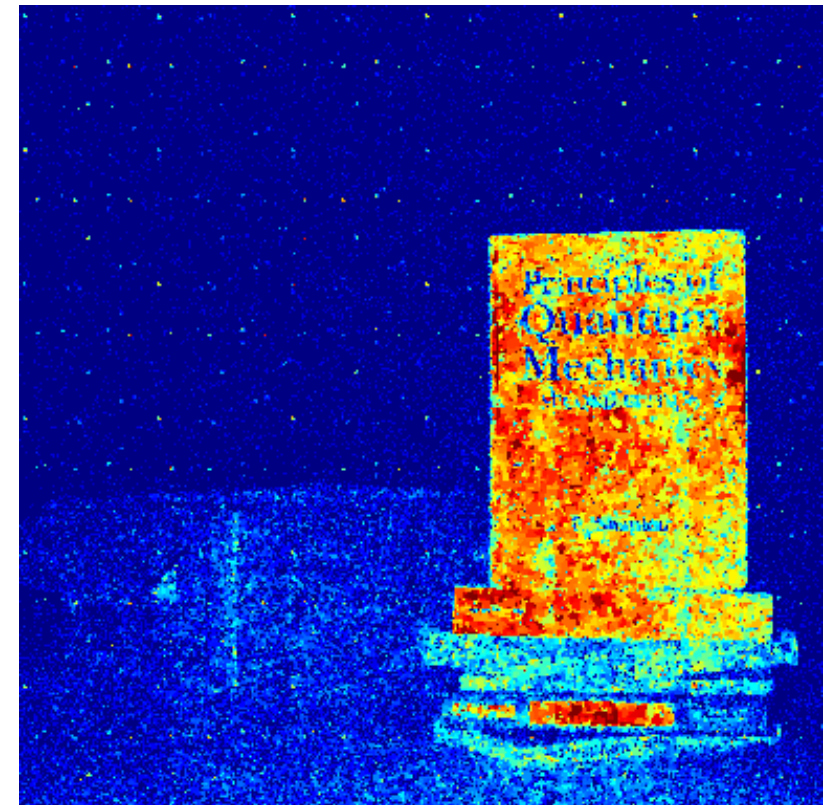
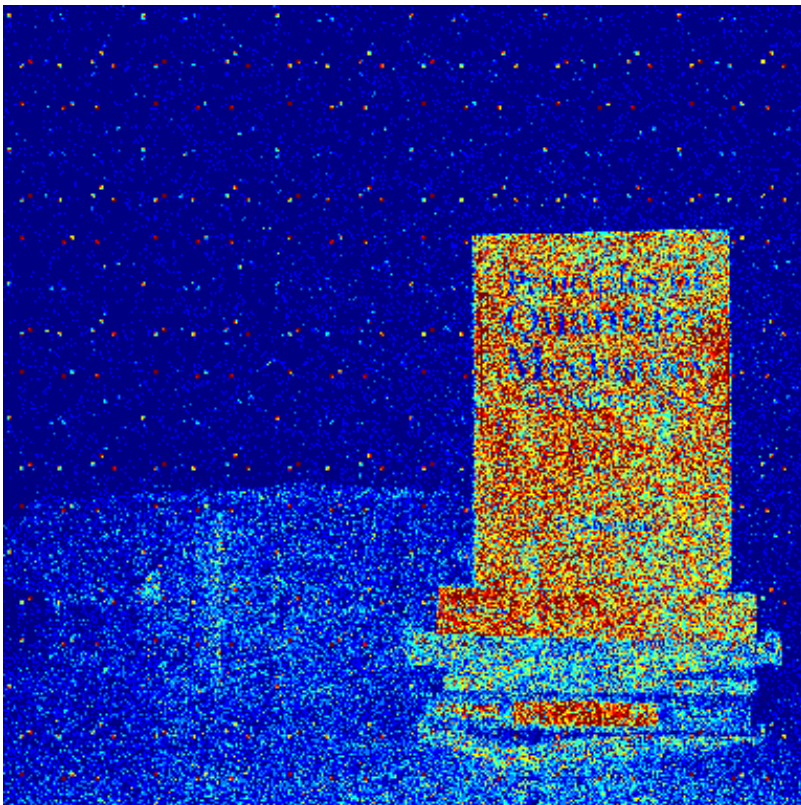
Results: Reflectivity

25 frames



Results: Reflectivity

50 frames



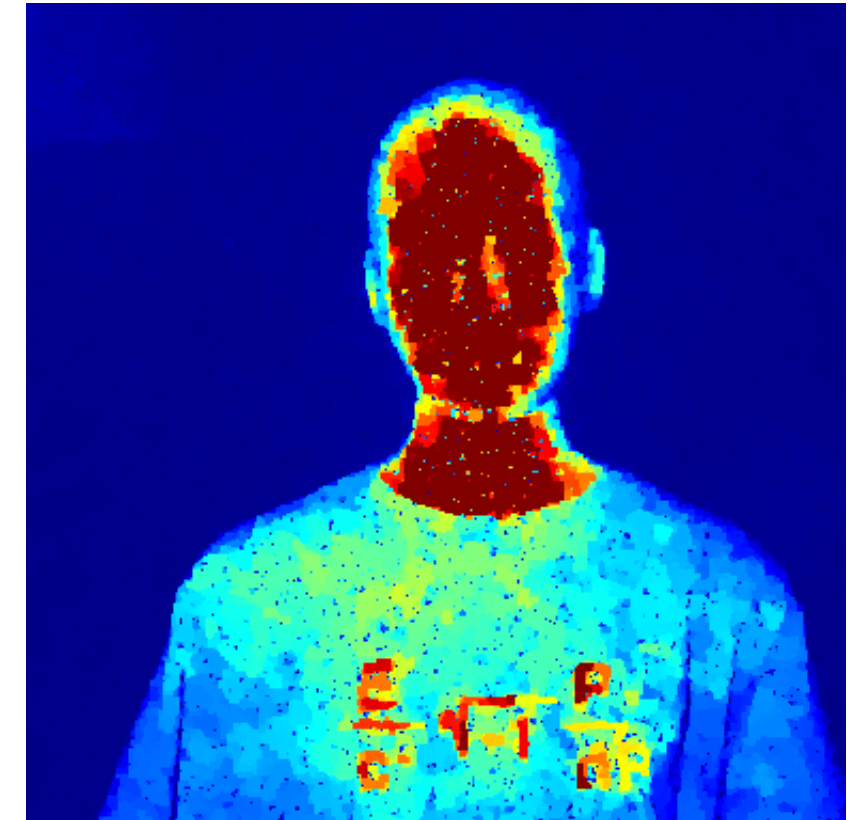
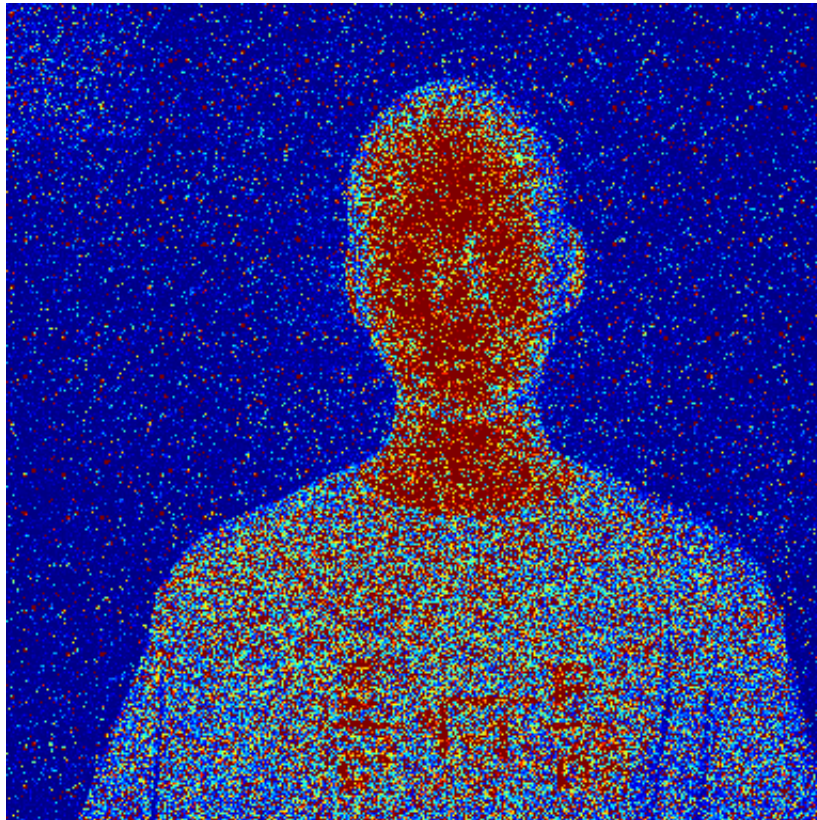
Results: Reflectivity

Results not as striking as first-photon imaging

- » Fixed-dwell time severely impacts dynamic range
- » Many pixels with no detection events
- » Need global long dwell times to get any detections in dark regions
- » Traditional averaging begins to work well for longer dwell times

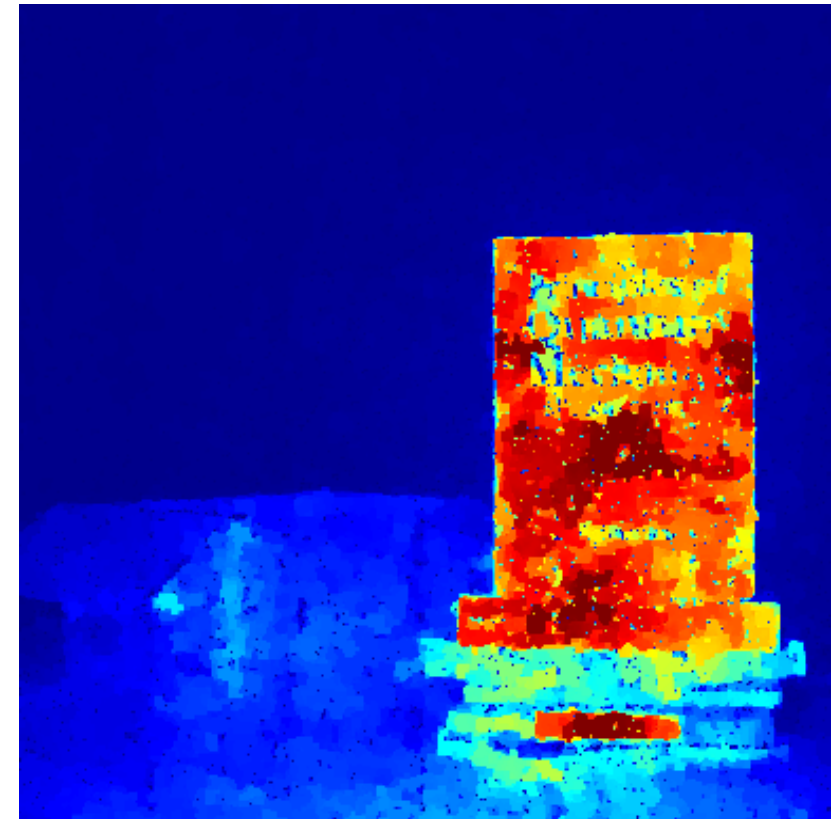
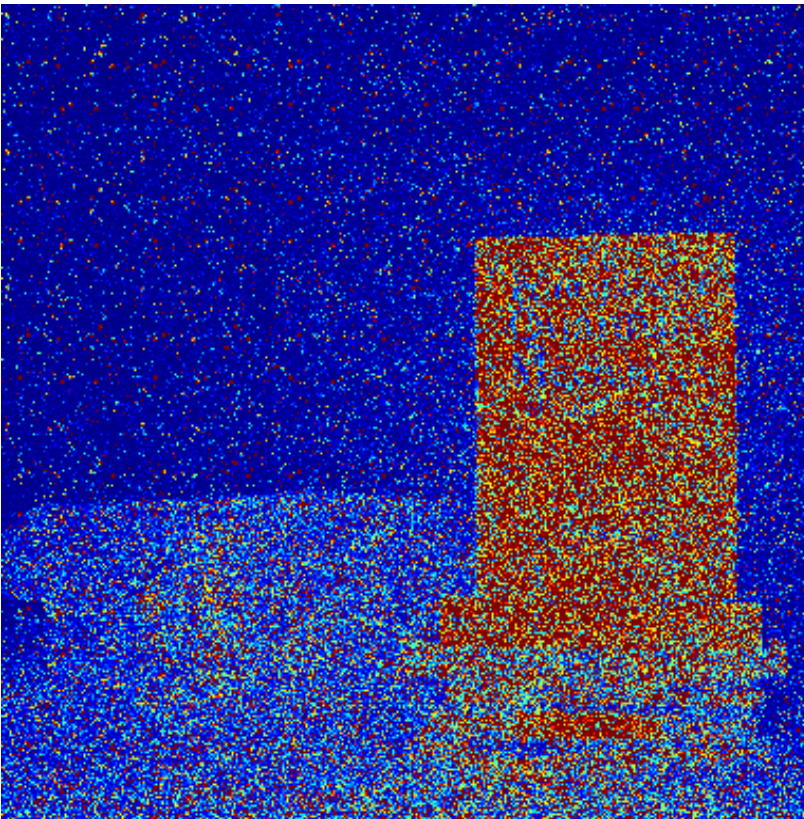
Results: Reflectivity

Simulated FPI



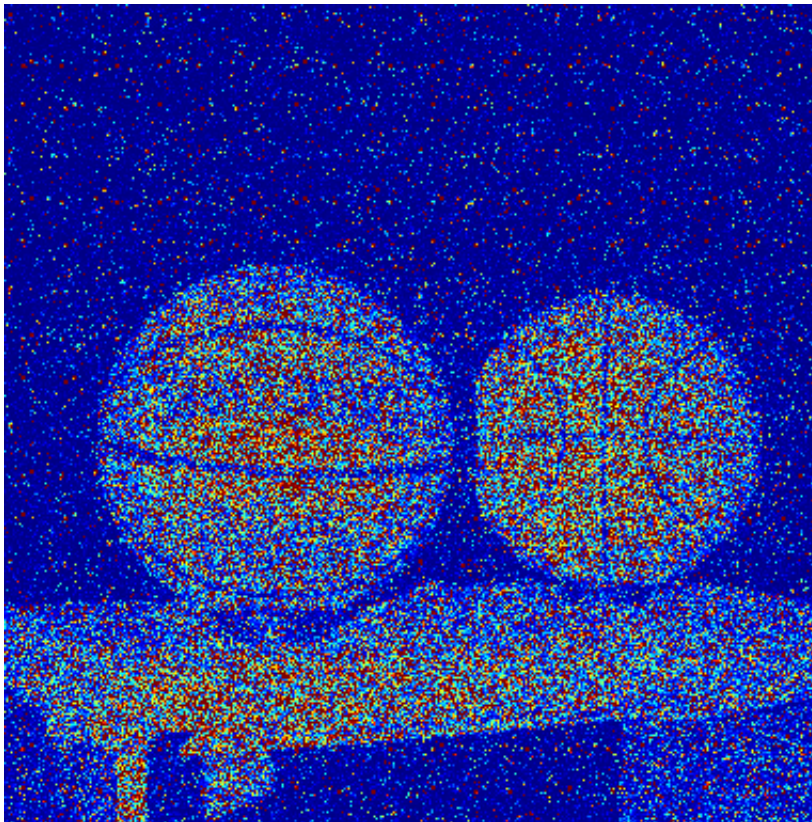
Results: Reflectivity

Simulated FPI



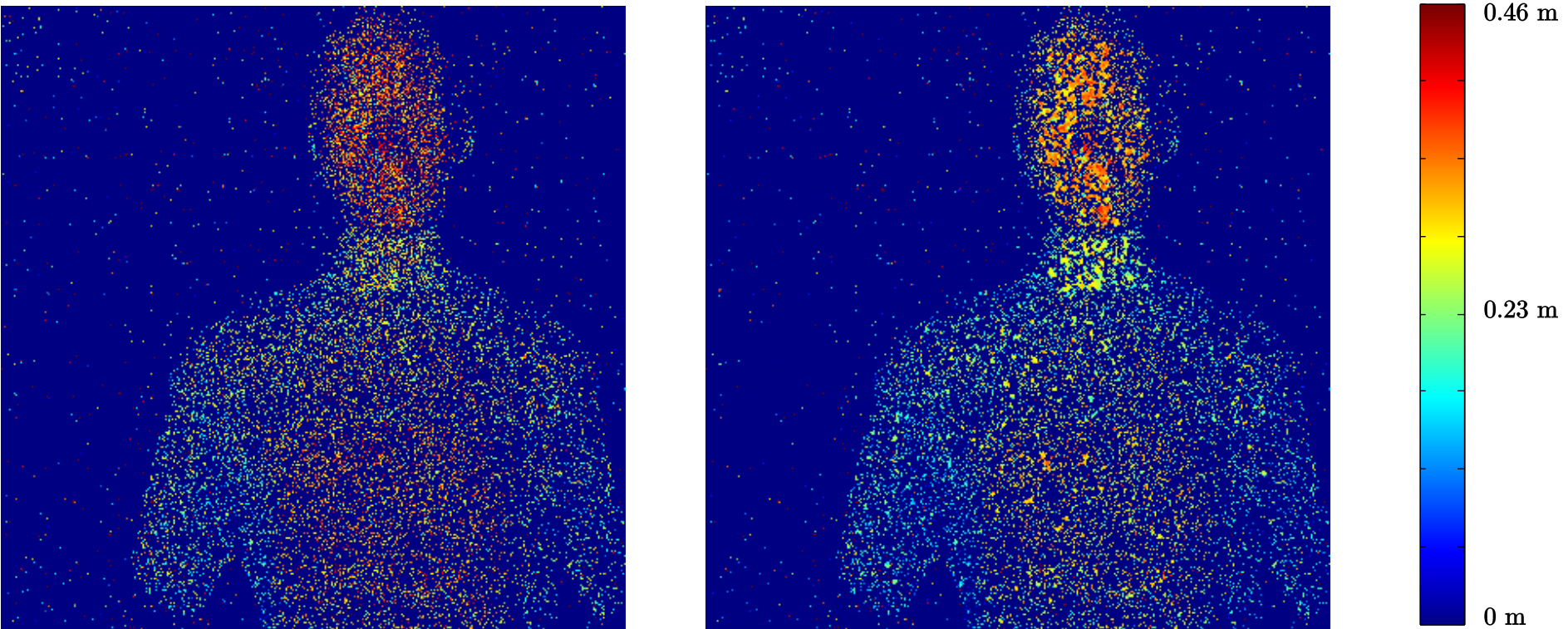
Results: Reflectivity

Simulated FPI



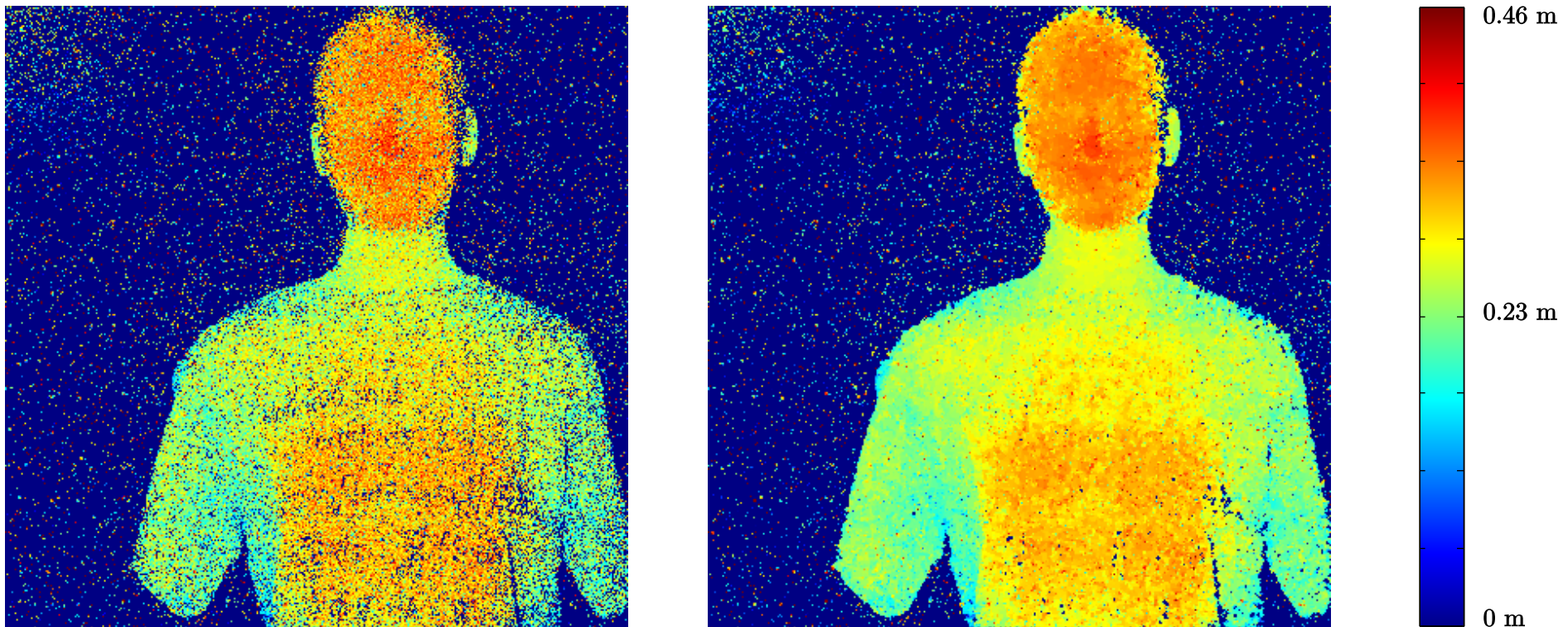
Results: Depth

25 frames



Results: Depth

400 frames



Results: Depth

Mismatch of laser pulse, object features, and time bin size

- » FPI: time bin (8 ps) < features (~50 ps) < pulse width (226 ps)
- » SPAD: time bin (389.9 ps) > pulse width (226 ps) > features (~50 ps)

Future experiments:

- » Change illumination to 1-2 ns pulse width
- » Change object to large, several-meter sized objects
- » SPAD arrays with improved time resolution

5 CONCLUSIONS

PC-OCT conclusions

Built classical phase-sensitive source

- » Amplified SPDC in entanglement-breaking regime

Implemented PC-OCT

- » Factor-of-2 resolution improvement as seen in Q-OCT
- » Even-order dispersion cancellation as seen in Q-OCT
- » Much faster acquisition possible with classical illumination/detection

GI conclusions

Built a second classical phase-sensitive source

- » Using 50/50 beamsplitter and a pair of SLMs
- » Computer-driven with deterministic, pseudorandom phase patterns
- » Capable of both phase-insensitive and phase-sensitive operation

Implemented phase-sensitive classical far-field GI

- » Inverted image as seen in biphoton-based GI
- » High-speed acquisition with classical illumination and detection

GI conclusions

Implemented computational GI

- » Reference arm replaced with computational simulation

Implemented compressive GI

- » Factor-of-10 speedup by assuming object is spatially sparse

Explored computational + compressive GI

- » Need SLM with more predictable operation
- » Limitations on use of compressive sensing

Single-photon imaging conclusions

First-photon imaging

- » Established collaboration with STIR group at MIT
- » Used techniques similar to compressed sensing to acquire high-quality depth and reflectivity images using 1 photon per pixel
- » Factor-of-100 speedup from traditional active imagers
- » Factor-of-10 sub-pulse depth resolution
- » 3-4 bit intensity resolution

Single-photon imaging conclusions

SPAD array imaging

- » Established collaboration with Zappa group at PdM
- » Adapted FPI algorithm to fixed dwell time case
- » Acquired and processed initial set of data
- » Reflectivity shows improvements but dynamic range limited
- » Depth images need larger objects and/or a longer pulse to show improvements using algorithm

Acknowledgements

Advisors / Thesis committee

Franco N. C. Wong, Jeffrey H. Shapiro, Vivek K. Goyal

Collaborators

Ahmed Kirmani, Andrea Colaço, Dongeek Shin, Rudi Lussana, Franco Zappa, Julien Le Gouët

Group members

Zheshen Zhang, Sara Mouradian, Murphy Niu, Valentina Schettini, Maria Tengner, Raúl García-Patrón, Veronika Stelmakh, Tian Zhong, Taehyun Kim, Onur Kuzucu, Saikat Guha, Nicholas Hardy, Baris Erkmen

Funding agencies

DARPA Quantum Sensing program, US Army Research Office, DARPA InPho program, National Science Foundation